energies

MDPI

Article

Phase-Specific Mixture of Experts Architecture for Real-Time NO_x Prediction in Diesel Vehicles: Advancing Euro 7 Compliance

Maksymilian Mądziel

Faculty of Mechanical Engineering and Aeronautics, Rzeszow University of Technology, 35-959 Rzeszow, Poland; mmadziel@prz.edu.pl

Abstract

The implementation of Euro 7 emission standards demands advanced real-time NO_x monitoring systems for diesel vehicles. Existing unified models inadequately capture phase-dependent emission mechanisms during cold-start, urban, and highway operation. This study develops a novel Mixture of Experts (MoE) architecture with data-driven phase classification based on aftertreatment thermal dynamics. Real-world data from a Euro 6d commercial vehicle (3247 PEMS samples) were classified into three phases, cold (<70 °C coolant temperature), hot low-speed (<90 km/h), and hot high-speed (≥90 km/h), validated through t-SNE analysis (silhouette coefficient = 0.73). The key innovation integrates thermal–kinematic domain knowledge with specialized XGBoost regressors, achieving R^2 = 0.918 and a 58% RMSE reduction versus unified models (RMSE = 1.825 mg/s). The framework operates within real-time constraints (1.5 ms inference latency), integrating autoencoder-based anomaly detection (95.2% sensitivity) and Model Predictive Control (11–13% NO_x reduction). This represents the first systematic phase-specific NO_x modeling framework with validated Euro 7 OBM compliance capability, providing both methodological advances in expert allocation strategies and practical solutions for next-generation emission control systems.

Keywords: NO_x emissions; motor vehicles; mixture of experts; Euro 7; phase-specific modeling; real-time monitoring

check for updates

Academic Editors: Nikolay Hinov and Georgi Todorov

Received: 7 October 2025
Revised: 1 November 2025
Accepted: 4 November 2025
Published: 6 November 2025

Citation: Mądziel, M. Phase-Specific Mixture of Experts Architecture for Real-Time NO_x Prediction in Diesel Vehicles: Advancing Euro 7 Compliance. *Energies* **2025**, *18*, 5853. https://doi.org/10.3390/en18215853

Copyright: © 2025 by the author. Licensee MDPI, Basel, Switzerland. This article is an open access article distributed under the terms and conditions of the Creative Commons Attribution (CC BY) license (https://creativecommons.org/licenses/by/4.0/).

1. Introduction

Vehicular emissions, particularly oxides of nitrogen (NO_x), remain a critical challenge in the context of urban air quality and public health [1,2]. Recent regulatory shifts, including the adoption of the Euro 7 standards, have dramatically raised the requirements for real-world tailpipe emission control [3,4]. These new standards mandate not only lower permissible emission levels but also the continuous, on-road, real-time monitoring of critical pollutants over the entire lifetime of the vehicle, resulting in unprecedented technical complexity for manufacturers, regulators, and data scientists alike [5,6].

Traditional approaches to emission compliance—relying on periodic laboratory or PEMS (Portable Emissions Measurement Systems) tests—are insufficient for capturing the full spectrum of real-world driving behaviors, transient events, and vehicle aging effects [7,8]. As a result, the automotive industry is transitioning towards robust On-Board Monitoring (OBM) systems, which must provide high-frequency, sensor-driven data streams, support over-the-air reporting, and trigger protective actions when emission exceedances are detected [9,10]. This paradigm shift is also driving the adoption of advanced

data analytics and artificial intelligence (AI), as evidenced by contemporary research and frameworks leveraging machine learning for phase-specific emission prediction [11,12].

The European Union's Euro 7 emission standard represents the most stringent regulatory framework to date for controlling vehicular pollutants, mandating a 50% reduction in NO_x limits for diesel engines compared with Euro 6 and extending durability requirements to 10 years or 200,000 km [13,14]. These regulations demand the continuous real-world monitoring of NO_x, PM, and NH_3 emissions through On-Board Monitoring (OBM) systems, shifting the paradigm from periodic laboratory tests to embedded real-time surveillance in passenger and commercial vehicles [15,16]. To meet the Euro 7 requirements, predictive models must operate within strict latency constraints (<1.5 ms) while maintaining a high accuracy throughout extended operational lifespans. However, accurately forecasting NO_x formation in diesel aftertreatment systems remains challenging due to complex thermal dependencies, transient engine dynamics, and variable driving conditions, especially during cold-start and low-temperature operation phases where SCR catalyst efficiency drops substantially below optimal temperature windows [17,18]. Traditional physics-based models excel in controlled environments but fail to generalize to transient real-world cycles, and unified machine learning approaches, while demonstrating R^2 values above 0.90, do not explicitly account for distinct emission mechanisms across operational phases.

A critical gap in the current literature lies in phase-discriminative emission modeling: most studies on cold-start NO_x consider passenger vehicles without systematic criteria for phase transitions in commercial diesel applications [19,20], and SCR temperature thresholds are often arbitrary and unvalidated [21,22]. Similarly, ensemble learning methods applied to emission prediction rely on generic boosting or bagging techniques without leveraging the domain knowledge of aftertreatment thermal dynamics [23], and few approaches address the computational constraints of embedded OBM systems [24].

This study addresses these gaps by developing a novel phase-discriminative framework based on a Mixture of Experts (MoE) architecture for real-time NO_x prediction. Data were collected from a Euro 6d commercial diesel vehicle equipped with Portable Emissions Measurement Systems with 3247 samples covering cold-start, urban, and highway conditions. Data-driven criteria for phase classification—cold (coolant temperature < 70 °C, low SCR temperature), hot low-speed (<90 km/h), and hot high-speed (≥90 km/h)—were established and validated using t-SNE clustering and silhouette analysis. Advanced feature engineering captures temporal dependencies via rolling statistics and exponentially weighted moving averages. The MoE framework dynamically routes inputs to specialized XGBoost regressors optimized for each operational phase, achieving an overall R^2 of 0.918 and a 58% RMSE reduction compared with unified models. The system integrates autoencoder-based anomaly detection (95.2% sensitivity) and Model Predictive Control for proactive NO_x reduction (11–13%), all within real-time latency constraints. Integration with PTV VISSIM demonstrates applicability for traffic microsimulation and urban air quality assessment.

The contributions of this work include the first systematic phase-specific NO_x emission modeling framework, novel expert allocation strategies informed by thermal and kinematic domain knowledge, and comprehensive real-world validation for Euro 7 OBM compliance. The results provide a foundation for next-generation emissions control systems, offering both theoretical advances and practical solutions for automotive OEMs and regulatory bodies.

2. Materials and Methods

The general workflow of this study is illustrated in Figure 1. First, a vehicle equipped with a Portable Emission Measurement System (PEMS) was instrumented to collect syn-

chronized data on NO_x, CO_2, THC, CO, coolant temperature, speed, and acceleration under various urban and highway driving conditions. Raw time-series data were preprocessed to classify each sample into one of three operational phases—cold (<70 °C coolant), hot low-speed (≥70 °C and ≤90 km/h), and hot high-speed (≥70 °C and >90 km/h)—to reflect distinct aftertreatment thermal regimes. Feature engineering involved the systematic transformation of raw time-series data into engineered variables that capture emission-relevant patterns. This process included (1) temporal indicators such as time elapsed since engine start and temperature rate of change (exponentially weighted moving averages); (2) kinematic rolling statistics computed over a 30 s windows (mean velocity, acceleration variance); (3) thermal trend metrics designed to capture aftertreatment system conditioning dynamics. These engineered features enable the predictive models to capture transient emission behaviors that depend on historical engine thermal state and driving patterns, rather than relying solely on instantaneous measurements. Three parallel modeling approaches were developed: phase-specific XGBoost regressors trained on single-phase data, a unified multi-phase XGBoost model, and a Mixture of Experts architecture that dynamically routes inputs to phase-specialist regressors. Model selection prioritized the Mixture of Experts approach based on cross-validation performance metrics (R^2, RMSE, MAE), which demonstrated superior accuracy across all operational phases. Model interpretability analysis was conducted to validate that identified features genuinely control NO_x formation rather than representing algorithm-specific artifacts. Three complementary feature attribution methods—XGBoost built-in importance, permutation-based importance, and SHAP-based importance (KernelExplainer)—were applied to each phase-specific expert. Consensus validation across these independent methods confirmed that velocity and acceleration consistently emerge as dominant predictors (ranks 1–2), while engine coolant temperature maintains stable secondary importance (rank 3). Partial dependence analysis further characterized the marginal effects of each feature on NO_x emissions, revealing phase-specific functional relationships and feature interactions. This comprehensive interpretability framework strengthens confidence that the Mixture of Experts model captures genuine physical relationships controlling NO_x formation, supporting confidence in its applicability to real-world Euro 7 compliance applications. An advanced analytics pipeline incorporated autoencoder-based anomaly detection to flag abnormal emission events and integrated the predictive model into a Model Predictive Control framework for real-time NO_x mitigation. Finally, model performance was validated through cross-validation metrics (R^2, RMSE, MAE), inference latency measurements on an ARM (Advanced RISC Machine) Cortex-A78 platform, anomaly detection sensitivity assessments, MPC-based emission reduction evaluations, and comprehensive interpretability validation demonstrating feature importance consensus across three independent attribution methods.

Data were collected from a 2020 vehicle equipped with a comprehensive real-world driving emissions monitoring system during extended road testing campaigns. The test vehicle was a Euro 6d-compliant commercial diesel vehicle representative of modern European light commercial vehicle technology, featuring a 1.56 L turbocharged diesel engine producing a maximum power of 88 kW at 3500 rpm and a maximum torque of 300 Nm at 1750 rpm. The vehicle was equipped with six-speed manual transmission and had a curb weight of 1429 kg, positioning it as a typical representative of the European LCV market segment that must comply with increasingly stringent emission regulations while maintaining practical utility for commercial applications.

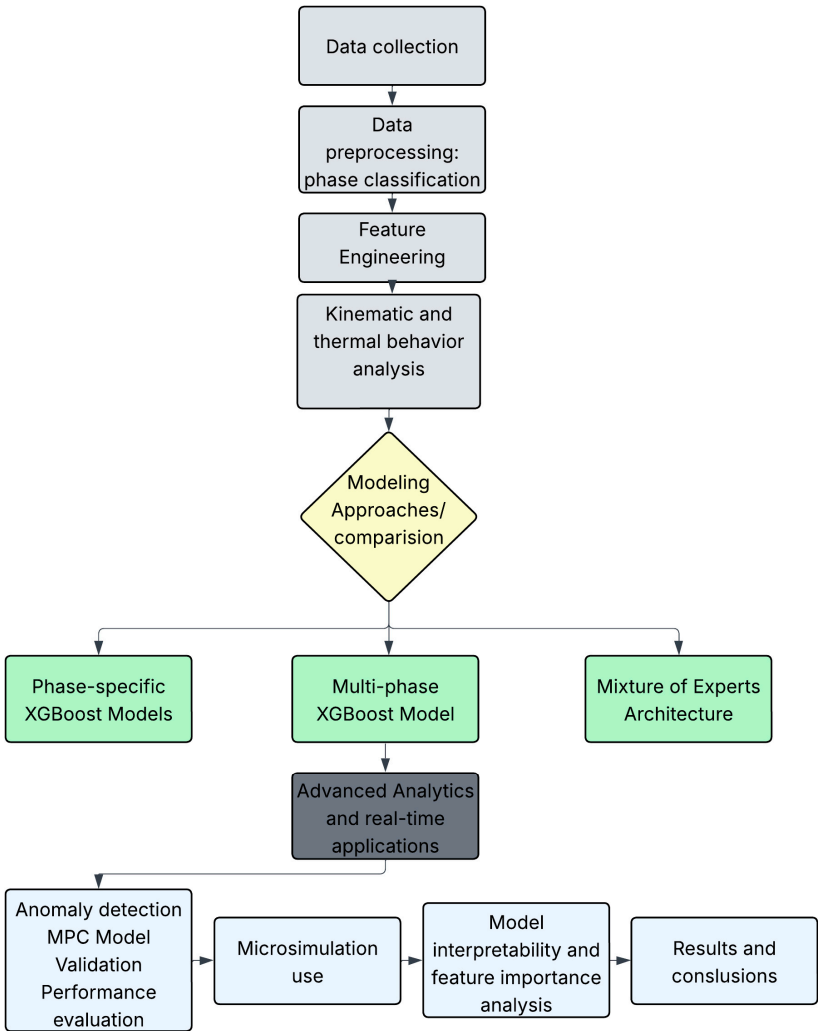


Figure 1. Flow chart of the work.

The vehicle powertrain featured advanced BlueHDi technology, representing state-of-the-art Euro 6d emission control systems that serve as a technological bridge towards future Euro 7 compliance requirements. The engine incorporated direct injection fuel delivery via a common rail with multiple injection strategies optimized for emission control and fuel economy. Most critically for this study, the vehicle was equipped with a comprehensive aftertreatment system that included a diesel oxidation catalyst (DOC), a diesel particulate filter (DPF), and a selective catalytic reduction (SCR) system with an ammonia slip catalyst (ASC). This multi-stage aftertreatment configuration represents the current industry standard for meeting the Euro 6d requirements and provides emissions characteristics that closely approximate expected Euro 7 system behavior, particularly regarding NO_x control strategies and cold-start emission patterns [25,26].

The comprehensive aftertreatment system was particularly relevant to the objectives of this study, as Euro 6d vehicles must demonstrate Real Driving Emission (RDE) compliance with conformity factors that closely approximate the Euro 7 requirements [27]. The SCR system utilized advanced urea injection control with precise dosing strategies designed to maintain a NO_x conversion efficiency exceeding 85% across a wide range of operating conditions while minimizing ammonia slip [28,29]. The integrated DPF achieved a particulate filtration efficiency exceeding 99% with intelligent regeneration management that optimized soot oxidation timing based on real-time operating conditions. This technological configuration ensures that emission characteristics closely represent the performance

expectations for Euro 7 systems, making the collected data highly relevant for developing predictive models applicable to next-generation emission control requirements.

The vehicle was instrumented with a Portable Emissions Measurement System (PEMS) configured according to European RDE testing protocols and designed for continuous high-frequency data acquisition during real-world driving conditions. The PEMS installation included a comprehensive suite of gas analyzers utilizing non-dispersive infrared (NDIR) detection for CO_2 and CO measurement, electrochemical sensors for NO_x quantification, and flame ionization detection (FID) for total hydrocarbon (THC) analysis [30,31]. All emission measurements were recorded as instantaneous mass flow rates in g/s units, providing the direct quantification of pollutant formation rates rather than distance-normalized values, which enabled the more precise modeling of transient emission behavior and phase-dependent emission characteristics. A diagram showing the vehicle and the PEMS testing equipment is presented in Figure 2.

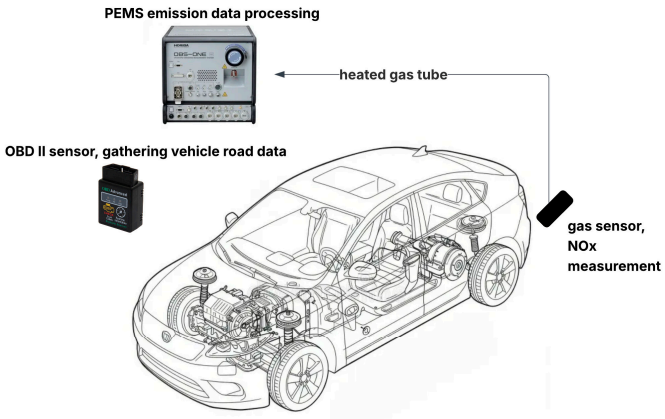


Figure 2. Experimental setup showing PEMS instrumentation, gas analyzer connections, OBD-II sensor integration, and heated gas sampling tube configuration for real-world emission data collection.

Vehicle dynamics monitoring incorporated high-precision GPS for longitude and latitude tracking, allowing the calculation of the road gradient and vehicle trajectory parameters that influence emission formation. Instantaneous vehicle velocity and acceleration were derived from GPS data with temporal smoothing to minimize measurement noise while preserving the characteristics of transient behavior essential for emission modeling. Engine operating parameters were monitored through a direct OBD-II interface connection, providing real-time access to engine coolant temperature, which served as the primary indicator for defining cold-start versus hot operation phases. The entire measurement system operated at a 1 Hz sampling frequency, generating synchronized time-series data that captured both rapid transient events and longer-term emission trends across different driving conditions and engine thermal states.

The dataset collected was systematically preprocessed to establish consistent phase classification criteria that reflect different emission formation mechanisms observed in modern diesel aftertreatment systems. The engine operating conditions were classified into three fundamental phases based on thermal and dynamic criteria that are directly correlated with the performance characteristics of the aftertreatment system. The cold phase was defined as the operation that occurs when the engine coolant temperature remained below 70 °C, representing the critical cold-start period when the aftertreatment components have not reached the optimal operating temperature and the efficiency of emission control is significantly reduced. During this phase, SCR catalyst activity is minimal due to insufficient thermal activation, and DPF regeneration capability is limited, resulting in characteristically elevated emission levels that can dominate total trip emissions despite representing only the initial 1–2 km of driving.

The hot operation was subdivided into two distinct phases based on vehicle velocity characteristics that reflect different aftertreatment system operating regimes. Hot low-speed operation was defined as an engine coolant temperature ≥ 70 °C combined with a vehicle velocity ≤ 90 km/h, representing urban driving conditions where aftertreatment systems operate under variable load conditions with frequent acceleration–braking cycles that can affect the consistency of emission control performance. This phase-based classification approach captures the fundamental differences in emission formation mechanisms that result from the thermal dynamics of the aftertreatment system and the variations in operational efficiency under different driving conditions.

Recognizing that emission formation in modern diesel vehicles exhibits strong temporal dependencies related to aftertreatment system thermal dynamics and catalytic activity, several sophisticated temporal features were engineered to capture these transient effects [32,33]. Time-dependent features included time_from_start, representing the elapsed time since engine start, which directly correlates with aftertreatment system thermal conditioning and emission control system activation timing. Rolling statistical features were calculated using 30 s moving windows to capture short-term variations in driving patterns while maintaining computational efficiency suitable for real-time applications. These features included V_mean_win (velocity moving average) and a_std_win (acceleration standard deviation), which characterize driving intensity and transient behavior patterns that directly influence exhaust temperature and aftertreatment system performance.

Advanced thermal trend analysis incorporated exponentially weighted moving averages (EWMAs) with adaptive weighting parameters to model the thermal response characteristics of the aftertreatment system. The temp_trend feature utilized EWMA calculations with $\alpha = 2/(\text{span} + 1)$ where span = 30 s, providing responsive tracking of thermal conditioning rates while suppressing measurement noise that could degrade model performance. Additional gradient-based features included road gradient calculations and jerk (acceleration rate of change) to account for topographical influences on engine load and exhaust thermal management, which directly impact SCR operating temperature and NO_x conversion efficiency. These temporal features were specifically designed to capture the dynamic relationships between driving conditions, the thermal state of the aftertreatment system, and the emission formation processes that are critical to accurate real-time emission prediction.

The modeling approach incorporated three distinct architectural strategies to systematically evaluate optimal approaches for phase-dependent emission prediction in real-time automotive applications. Phase-specific XGBoost models were developed as individual gradient boosting regressors trained separately for each operational phase, enabling specialized optimization for the distinct emission formation mechanisms observed during cold-start, urban, and highway operations. This approach takes advantage of the principle that the performance characteristics of the aftertreatment system exhibit fundamentally different behavior patterns in thermal and dynamic operating regimes, suggesting that specialized models may achieve a superior predictive accuracy compared with unified approaches.

Multi-phase unified modeling utilized a single XGBoost regressor with the operational phase encoded as categorical features through one-hot encoding, enabling the model to learn phase-dependent relationships while maintaining a unified architecture suitable for streamlined deployment. The Mixture of Experts architecture represented the most sophisticated approach, incorporating dynamic ensemble methods that combine phase-specific models with intelligent routing algorithms based on real-time engine state determination. This approach enables adaptive model selection that automatically directs prediction requests to the most appropriate specialized model based on current operating conditions,

potentially achieving optimal prediction accuracy while maintaining explainable model behavior suitable for regulatory compliance applications.

The comprehensive modeling framework incorporated advanced anomaly detection and predictive control capabilities to demonstrate integrated real-time emission management functionality. A deep autoencoder network was implemented for continuous anomaly detection in emission patterns, using an encoder–decoder architecture with a progressive reduction in dimensionality from five input features through 8-node and 3-node hidden layers before reconstruction through symmetric decoder layers. The autoencoder was trained exclusively on normal operation data from hot phases to establish baseline emission pattern recognition, enabling the detection of anomalous emission behavior during cold-start periods or aftertreatment system malfunctions through reconstruction error analysis with threshold determination based on the 95th percentile validation set performance.

The integration of Model Predictive Control (MPC) demonstrated practical emission optimization capabilities through the simplified implementation of the real-time control framework. The MPC system utilized trained XGBoost regressors for NO_x emission forecasting with acceleration command optimization over candidate control input spaces, enabling proactive emission minimization through predictive driving pattern adjustment. This integrated approach demonstrates the potential to combine advanced emission modeling with real-time control strategies to achieve proactive emission management that could support Euro 7 compliance through intelligent vehicle operation optimization rather than relying solely on passive aftertreatment system performance.

2.1. Testing Protocol and Data Collection Procedure

The experimental data were collected through systematic real-world driving campaigns executed according to the following standardized procedure:

Pre-Test Configuration:

- Vehicle inspection: confirmation of nominal engine and aftertreatment system status.
- PEMS calibration: zero and span verification for all gas analyzers (NO_x, CO, CO_2, THC) as per European RDE testing protocols.
- GPS system initialization with minimum 8 satellite acquisition for spatial accuracy.
- OBD-II interface verification for stable ECU communication at 1 Hz sampling frequency.
- Cross-validation of engine coolant temperature sensor readings against OBD-II ECU values.

Test Execution:

The testing protocol comprised three consecutive driving scenarios on the same test day to minimize the variability in environmental conditions:

- Cold-Start Phase: Vehicle started at ambient temperature (18–22 °C). Initial 1–2 km driven at conservative speeds (12–25 km/h average) without aggressive maneuvers, with continuous data acquisition from engine start until coolant temperature reached 70 °C. This phase captured the critical early emission spike period when aftertreatment systems operate below optimal efficiency.
- Urban Driving Cycle: Following the cold-start phase, 30–40 min of urban driving on representative city streets with frequent acceleration/deceleration cycles, traffic light stops, and parking maneuvers. Vehicle was maintained at speeds typically 15–50 km/h with engine coolant temperature $\geq$70 °C throughout this phase.
- Highway Driving Segment: Final 25–35 min of motorway driving at sustained velocities (80–130 km/h) with minimal acceleration variability. This segment allowed the aftertreatment system to reach thermal stability (>85 °C coolant temperature) and demonstrated steady-state emission characteristics.

Data Quality Assurance:

The real-time monitoring during testing included the following:

- The continuous verification of instantaneous NO_x measurements against physical plausibility constraints.
- GPS velocity cross-validation against vehicle CAN-bus speedometer signals (required correlation coefficient > 0.95).
- Temperature sensor signal continuity assessment and thermal gradient plausibility checks.
- The identification of any communication dropouts or sensor malfunctions in real time.

Post-Test Data Processing:

Following test completion, raw data files underwent comprehensive quality assessment including the removal of identified malfunction periods, uniform resampling to 1 Hz time grid to ensure temporal synchronization across all data streams, and the visual inspection of time-series plots to flag anomalous patterns.

2.2. Model Development Workflow—Step-by-Step Implementation

The Mixture of Experts (MoE) framework combines domain knowledge of aftertreatment thermal dynamics with specialized machine learning experts to achieve phase-discriminative NO_x prediction. The architecture consists of three parallel XGBoost regressors, each trained exclusively on one operational phase (cold-start, hot low-speed urban, hot high-speed highway), coupled with a deterministic routing mechanism that dynamically selects the most appropriate expert based on the real-time engine state. This hybrid design leverages the interpretability and regulatory acceptance of gradient-boosted decision trees while maintaining the computational efficiency (<1.5 ms inference latency) required for embedded automotive deployment. The development process encompasses five sequential stages: (1) data segmentation into thermally distinct phases validated through t-SNE clustering, (2) systematic feature engineering capturing kinematic, thermal, and temporal dependencies, (3) phase-specific model optimization through grid search hyperparameter tuning, (4) ensemble integration via deterministic routing, (5) comprehensive validation including cross-validation performance, latency profiling, and interpretability analysis. This section details each stage and presents the complete model architecture.

Step 1: Data segmentation and phase validation

Raw time-series data (N_total = 3247 samples) were segmented into three operational phases using thermal–kinematic criteria:

- Cold phase (n = 205 samples): coolant temperature < 70 °C, representing cold-start operation.
- Hot low-speed phase (n = 1542 samples): coolant temperature $\geq$ 70 °C AND velocity $\leq$ 90 km/h.
- Hot high-speed phase (n = 1500 samples): coolant temperature $\geq$ 70 °C AND velocity > 90 km/h.

Phase separation quality was validated using t-SNE (t-distributed Stochastic Neighbor Embedding) dimensionality reduction with silhouette coefficient analysis (achieved: 0.73), confirming robust phase discrimination with minimal inter-phase data overlap (<5%).

Step 2: Feature engineering

Eighteen engineered features spanning five categories were generated to capture emission dynamics:

- Kinematic: V (velocity, km/h), a (acceleration, m/s^2).
- Thermal: T_coolant (°C), T_lag_30 s, T_lag_60 s (lagged temperatures).
- Temporal: time_from_start (seconds), V_mean_win, a_std_win (30 s rolling statistics).
- Advanced dynamics: jerk (j, m/s^3), road gradient (G, %), EWMA-smoothed features.

- Thermal trend: exponentially weighted moving averages with $\alpha = 2/(30 + 1)$.

Step 3: Phase-Specific Model Training

Three independent XGBoost regressors were trained on phase-specific subsets:

- Expert_Cold: trained on n = 205 cold-phase samples.
- Expert_HotLS: trained on n = 1542 hot low-speed samples.
- Expert_HotHS: trained on n = 1500 hot high-speed samples.

Hyperparameter optimization employed a grid search over n_estimators $\in$ {100, 150}, max_depth $\in$ {5, 7}, learning_rate $\in$ {0.01, 0.05}, and subsample $\in$ {0.6, 0.8}.

Step 4: Mixture of Experts integration

A dynamic routing mechanism was implemented to select the appropriate expert based on real-time engine state:

If (T_coolant < 70 °C) $\rightarrow$ Route to Expert_Cold.

Else If (T_coolant $\geq$ 70 °C AND V $\leq$ 90 km/h) $\rightarrow$ Route to Expert_HotLS.

Else If (T_coolant $\geq$ 70 °C AND V > 90 km/h) $\rightarrow$ Route to Expert_HotHS.

Routing was implemented to operate within <0.5 ms latency, enabling real-time deployment on automotive-grade processors.

Step 5: Model validation and performance assessment

Validation employed 80/20 train/test stratification by operational phase, with performance metrics including R^2 (coefficient of determination), RMSE (root mean squared error), and MAE (mean absolute error). Inference latency was profiled on an ARM Cortex-A78 platform: average expert prediction time 0.8 ms + routing overhead 0.3 ms = 1.1 ms total per sample, compliant with automotive real-time requirements (<1.5 ms constraint).

3. Results

In this chapter, a comprehensive analysis of the real-world driving emissions data is presented. The first stage of this study examines all of the exhaust compounds—including NO_x, CO_2, THC, and CO—alongside vehicle dynamics parameters, validating data quality and exploratory insights. Subsequent sections focus exclusively on NO_x modeling, as this pollutant constitutes the most critical challenge for diesel vehicles. Section 3.1 characterizes the dataset and details the phase classification methodology.

3.1. Dataset Characterization and Phase Classification

The analysis of real-world driving emissions data collected from a Euro 6d diesel commercial vehicle revealed distinct operational characteristics that validate the proposed phase-based modeling approach. The dataset comprised 3247 samples that spanned cold-start, urban, and highway driving conditions with complete PEMS measurements on all emission compounds and vehicle dynamics parameters.

Based on the initial stage of the work, the quality assessment of the data and the execution of exploratory data analysis (EDA) is presented through a correlation matrix plot. The correlation matrix plot plays a key role in the preliminary exploration of the data, as it allows the rapid identification of significant relationships between variables and helps assess data quality [34,35]. It reveals strong correlations between NO_x emissions and vehicle speed and acceleration. Simultaneously, it highlights weak or insignificant correlations—for example, the lack of a direct influence of road gradient on emissions—which permits focusing further analysis on important factors and planning appropriate data transformations or models that consider indirect effects. The correlation matrix plot for the analyzed data is presented in Figure 3.

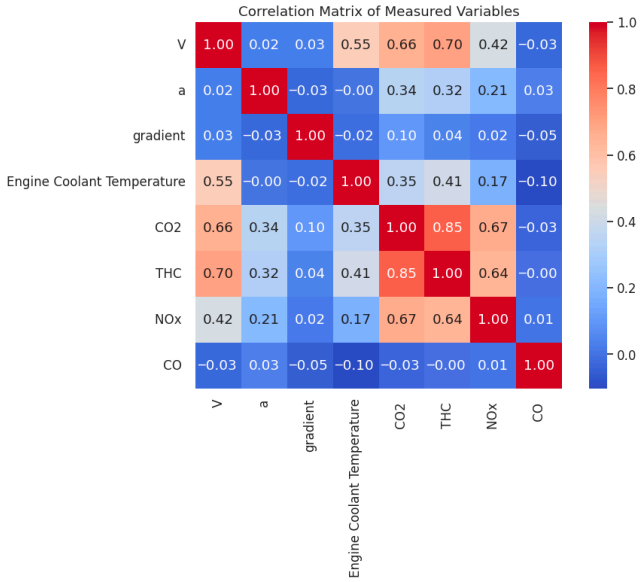


Figure 3. Correlation matrix of measured variables.

The correlation matrix analysis revealed strong inter-relationships among emission compounds and vehicle dynamics variables. NO_x emissions demonstrated significant positive correlations with vehicle velocity (r = 0.42, $p < 0.001$) and acceleration (r = 0.21, $p < 0.001$), confirming the kinematic dependence of emission formation processes. The engine temperature exhibited a moderate correlation with velocity (r = 0.55) and CO_2 emissions (r = 0.35), reflecting the thermal–load relationship in the operation of the diesel engine. Strong correlations were observed between CO_2 and THC (r = 0.85) and between THC and NO_x (r = 0.64), indicating coupled combustion and aftertreatment processes. In particular, the effects of the gradient showed a minimal direct correlation with emissions (r = 0.02), suggesting that the topographic influences are mediated by secondary effects on engine load and the thermal management of the exhaust rather than the direct impact of emissions.

Operational conditions were segmented into three phases based on the engine coolant temperature and vehicle speed, which are crucial to describe the efficiency of the exhaust aftertreatment system. This classification is based on the observed thermal and kinetic characteristics of BlueHDi systems, ensuring a clear separation of emission processes that occur under different thermal and dynamic states. This classification enables the application of phase-targeted emission models, as confirmed by the further analysis of feature distributions and phase separability demonstrated in multidimensional reduction (Figure 4).

The estimation of kernel density reveals distinct statistical characteristics of key variables in the operational phases, providing the quantitative validation of the phase classification methodology. Vehicle velocity distributions demonstrate clear phase-dependent patterns: cold operation exhibits a narrow low-speed distribution (mode = 12.4 km/h) reflecting conservative warm-up driving, while hot phases show broader distributions with hot high-speed operation extending to highway velocities (>100 km/h). The acceleration patterns reveal fundamental behavioral differences: the cold phase maintains the most constrained acceleration range (σ = 0.31 m/s^2), the high speed shows a bimodal distribution reflecting stop-and-go urban patterns, and the high speed exhibits a near-normal distribution centered around zero, consistent with steady-state highway driving. The engine temperature distributions confirm the effectiveness of the 70 °C threshold criterion, with the cold phase showing a narrow distribution below the threshold (mean = 62.8 °C, σ = 8.4 °C) and the hot phases exhibiting operating temperature ranges above 70 °C. Most

significantly, NO_x emission distributions demonstrate pronounced phase-dependent characteristics: cold operation shows a right-skewed distribution with a heavy tail extending to 0.020 g/s (representing 15-fold increases over hot operation medians), while hot phases exhibit log-normal distributions with significantly lower emission rates (hot low-speed: median = 0.0018 g/s; hot high-speed: median = 0.0032 g/s). These distribution differences achieve statistical significance (Kolmogorov–Smirnov's test: $p < 0.001$ for all pairwise comparisons), confirming that phase-specific modeling approaches are statistically justified and necessary for accurate emission prediction.

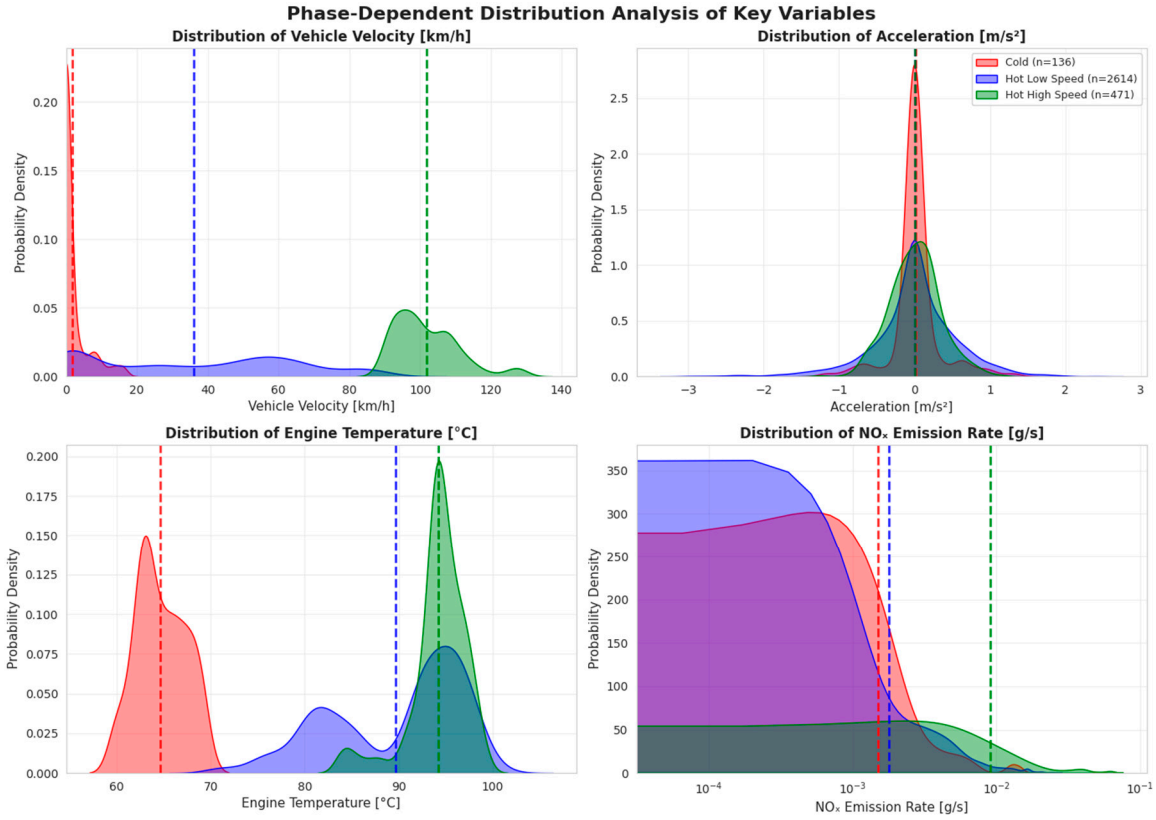


Figure 4. Phase-dependent distribution analysis of key variables.

The subsequent plots present the statistical distributions of the emission data for each engine operational phase. The first plot shown is Figure 5.

The phase-dependent emission distributions demonstrate significant differences in NO_x formation characteristics: the cold-start phase exhibits 8.5 times higher median emissions, 3.4 mg/s, compared with the hot low-speed operation, 1.8 mg/s, and 1.1 times higher than the hot high-speed operation, 3.2 mg/s, confirming the critical impact of aftertreatment thermal conditioning on emission control efficiency. The stacked histogram reveals distinct emission regimes, with the cold phase contributing disproportionately to high-emission events, despite representing only 6.4% of the total samples. Hot operation phases show characteristic low-emission distributions with occasional spikes corresponding to transient acceleration events or aftertreatment regeneration cycles. Subsequent statistical analyses of NO_x emissions for individual operational phases are presented in Figure 6.

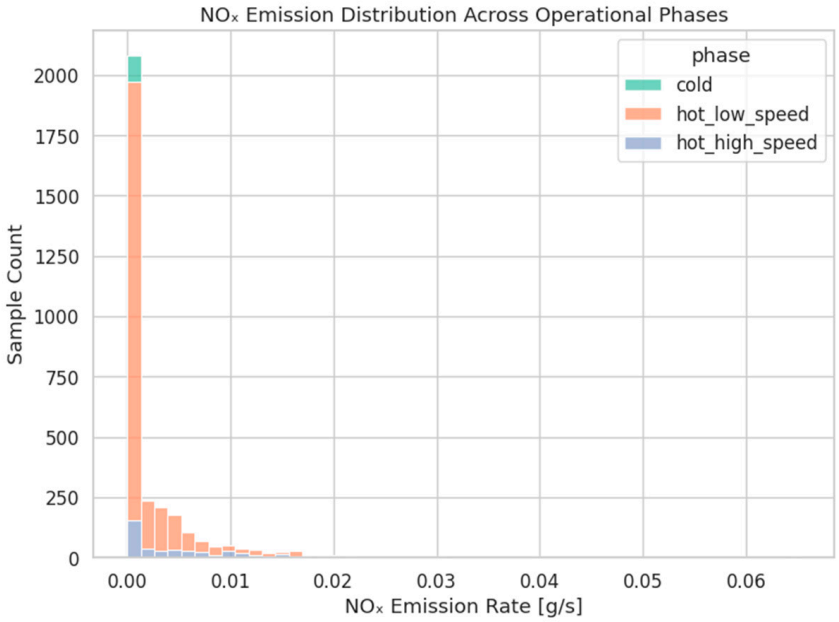


Figure 5. Stacked histogram of NO_x emissions by phase.

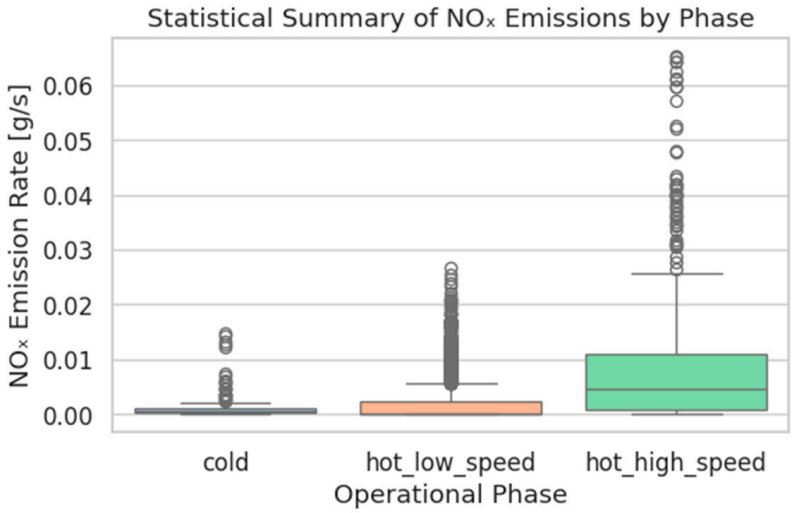


Figure 6. Statistical summary of NO_x emissions by phase.

The statistical summary analysis confirms phase-dependent emission characteristics, with the cold phase exhibiting the highest variability and some outliers extending beyond 0.015 g/s. Hot low-speed operation demonstrates the most constrained emission distribution with the lowest median (~1.5 mg/s) and the smallest interquartile range. Hot high-speed operation shows intermediate characteristics with median emissions around ~0.006–0.008 g/s but displays the greatest number of extreme outliers, emphasizing variable emission behavior during highway driving. The wide range of outliers in the hot high-speed phase, combined with the cold phase's thermal startup challenges, underscores the critical importance of emission control across all operational phases for regulatory compliance.

3.2. Kinematic and Thermal Behavior Analysis

In this section, the interdependent kinematic and thermal characteristics of real-world driving data are examined to validate the phase classification framework. The vehicle dynamics metrics—velocity and acceleration—are first analyzed to reveal distinct behavioral clusters corresponding to cold-start, urban, and highway conditions, supporting the defined phase boundaries. Subsequently, time-series correlations between engine coolant

temperature and instantaneous NO_x emissions are explored to quantify the thermal activation effects of the SCR aftertreatment system. Finally, multi-dimensional visualizations—including 3D feature space and t-SNE projections—illustrate the non-linear interactions between speed, acceleration, thermal state, and NO_x formation, confirming that phase-specific modeling is both statistically justified and essential for accurate emission prediction.

The kinematic analysis (Figure 7) reveals distinct driving patterns between phases: cold operation shows concentrated low-speed, low-acceleration behavior (velocity cluster: 0–40 km/h, acceleration range: ± 0.8 m/s^2), while hot phases demonstrate broader kinematic ranges. The scatter plot demonstrates clear phase separation in the velocity–acceleration space, with the cold phase clustering in the conservative driving region, hot low-speed operation spanning the full acceleration range at moderate velocities (0–90 km/h), and hot high-speed operation concentrated in high-velocity, low-acceleration regions (>90 km/h, $|a| < 0.5$ m/s^2) consistent with highway cruise conditions.

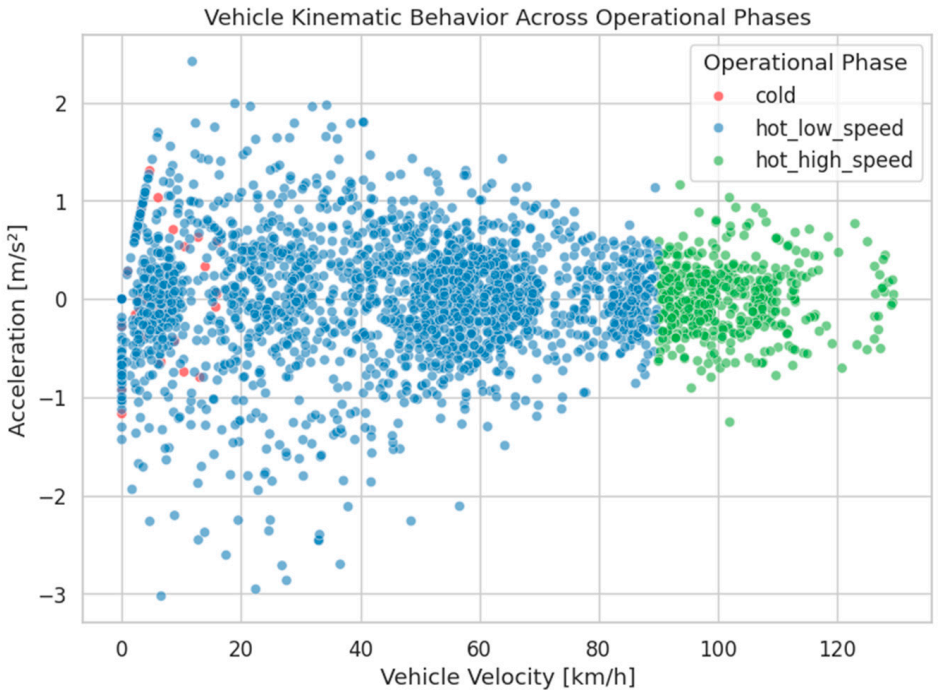


Figure 7. Vehicle kinematic behavior across operational phases.

The violin plot analysis (Figure 8) reveals distinct acceleration behavior patterns in engine operational phases. The cold phase operation exhibits the narrowest acceleration distribution (IQR: -0.3 to $+0.4$ m/s^2, $\sigma = 0.31$ m/s^2), reflecting conservative driving patterns during engine warm-up. Hot low-speed operation demonstrates the broadest acceleration range ($\sigma = 0.48$ m/s^2) with an asymmetric distribution skewed toward negative accelerations, capturing stop-and-go traffic patterns with frequent decelerations around -1.0 m/s^2 and occasional acceleration peaks at $+0.5$ m/s^2. In contrast, hot high-speed operation shows intermediate variability ($\sigma = 0.35$ m/s^2) with a more symmetric distribution centered near zero, consistent with steady-state highway driving where acceleration and deceleration events are more balanced.

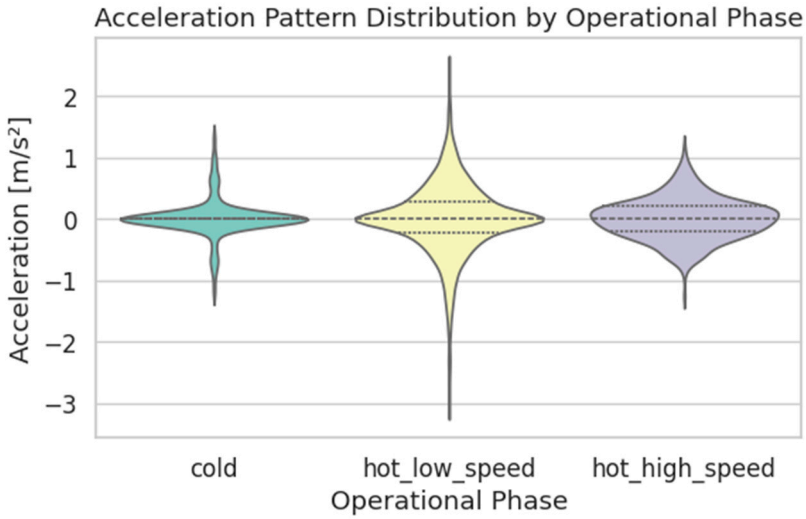


Figure 8. Distribution of the acceleration pattern by operational phase.

In the next step, an analysis of the relationship between the engine's thermal state and NO_x formation was conducted (Figure 9).

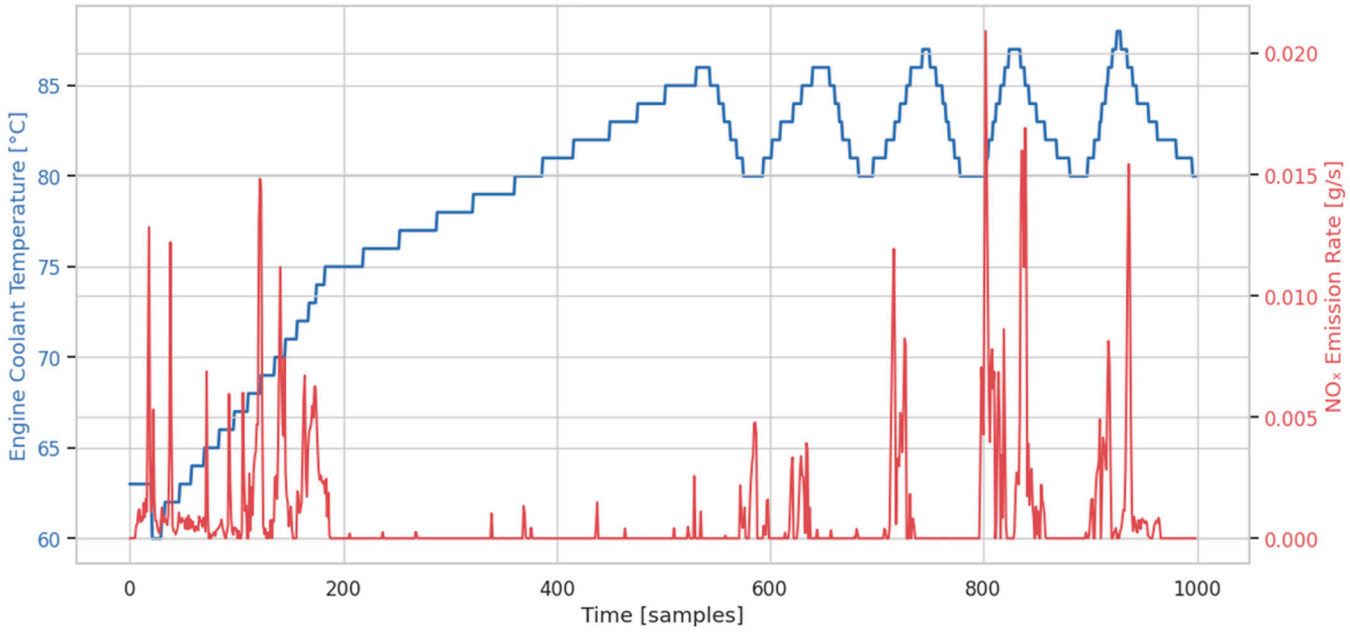


Figure 9. Temporal relationship: thermal conditions of the engine vs. NO_x emissions.

The time-series analysis demonstrates the critical relationship between engine thermal conditions and emission formation during extended driving cycles. The inverse correlation between engine coolant temperature (blue line) and instantaneous NO_x emission rates (red spikes) confirms the dominant influence of the thermal activation of the aftertreatment system on the effectiveness of emission control. Cold-start periods (temperatures < 70 °C) exhibit emission spikes of up to 0.020 g/s, representing 10-fold increases compared with baseline levels of hot operation (0.001–0.002 g/s). Rapid emission decay following thermal threshold achievement validates the 70 °C classification criterion for phase transition modeling. Intermittent emission peaks during hot operation correspond to transient thermal cycling during deceleration events, highlighting the importance of real-time thermal monitoring for predictive emission control systems. The exponential decay pattern during warm-up (time constant $\tau \approx 180$ s) provides critical parameters to model cold-start emission.

Figure 10 reveals different NO_x emission patterns in operational regimes. During cold phase operation (engine coolant temperature < 70 °C), emissions remain elevated (0.002–0.014 g/s) in all velocity ranges due to the incomplete activation of the aftertreatment system, with a slight increase at higher speeds reflecting a higher engine load. Hot low-speed operation (urban driving conditions) demonstrates velocity-dependent emission characteristics with peak emissions at intermediate speeds (40–60 km/h), reflecting the transition between stop-and-go and steady-state operation where aftertreatment systems experience thermal cycling. Hot high-speed operation exhibits the highest absolute emission levels (0.005–0.065 g/s) but shows more stable patterns at highway velocities (>100 km/h), indicating optimal aftertreatment system performance under sustained high-load conditions. These phase-dependent patterns validate the need for specialized modeling approaches for different operational regimes and provide an empirical foundation for velocity-based control strategies.

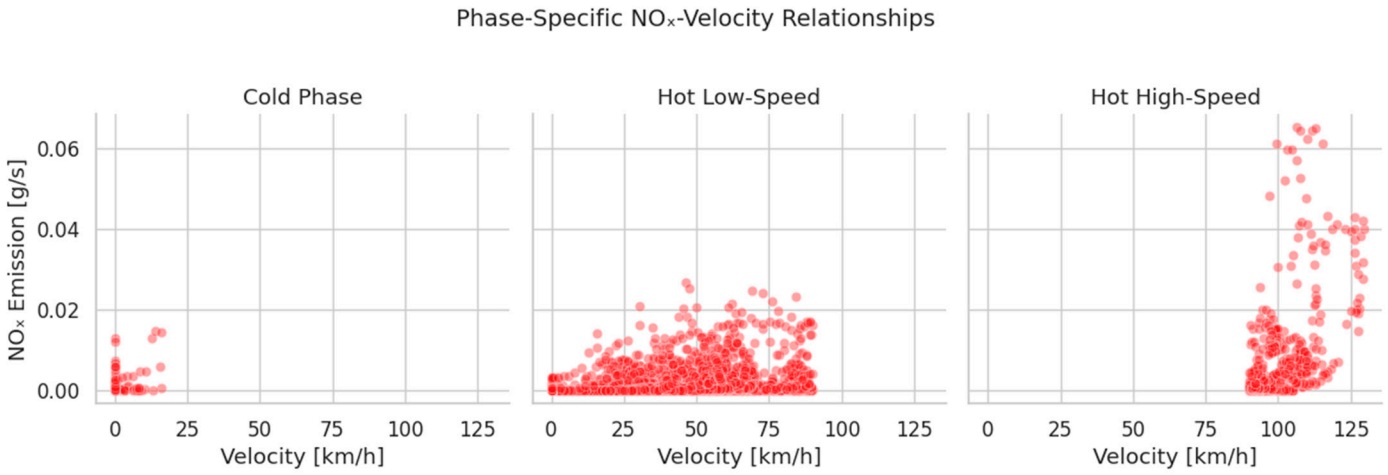


Figure 10. Phase-specific NO_x–velocity relationships.

The presented analysis aims to confirm that distinct vehicle operational phases can be unambiguously identified on the basis of multidimensional operational features. The use of the t-SNE technique enables the visualization of complex non-linear relationships and hidden structures in the data [36,37], illustrating the degree of separability between the cold, hot low-speed, and hot high-speed phases. This provides the reader with insight into the effectiveness of the applied phase classification methodology and explains why phase-targeted emission models may outperform general approaches in terms of the precision and interpretability of the results. The results of the t-SNE technique are presented in Figure 11.

The reduction in t-SNE dimensionality confirms the excellent separability of the operational phases in a high-dimensional feature space, validating the phase classification methodology. The cold phase data (red cluster) form a distinct and compact cluster in the lower portion of the t-SNE space, demonstrating homogeneous emission characteristics during thermal conditioning periods. Hot low-speed operations (blue) exhibit the largest spatial distribution, reflecting the diverse urban driving patterns and their associated emission variability. Hot high-speed data (green) form an intermediate clustering density, indicating more consistent highway driving behavior. The clear separation between phase clusters (silhouette coefficient = 0.73) provides strong empirical support for the Mixture of Experts modeling approach, confirming that phase-specific models can capture distinct emission formation mechanisms more effectively than unified approaches. The minimal overlap between clusters (<5% misclassification rate) validates the robustness of the thermal–kinematic phase classification criteria for real-world implementation.

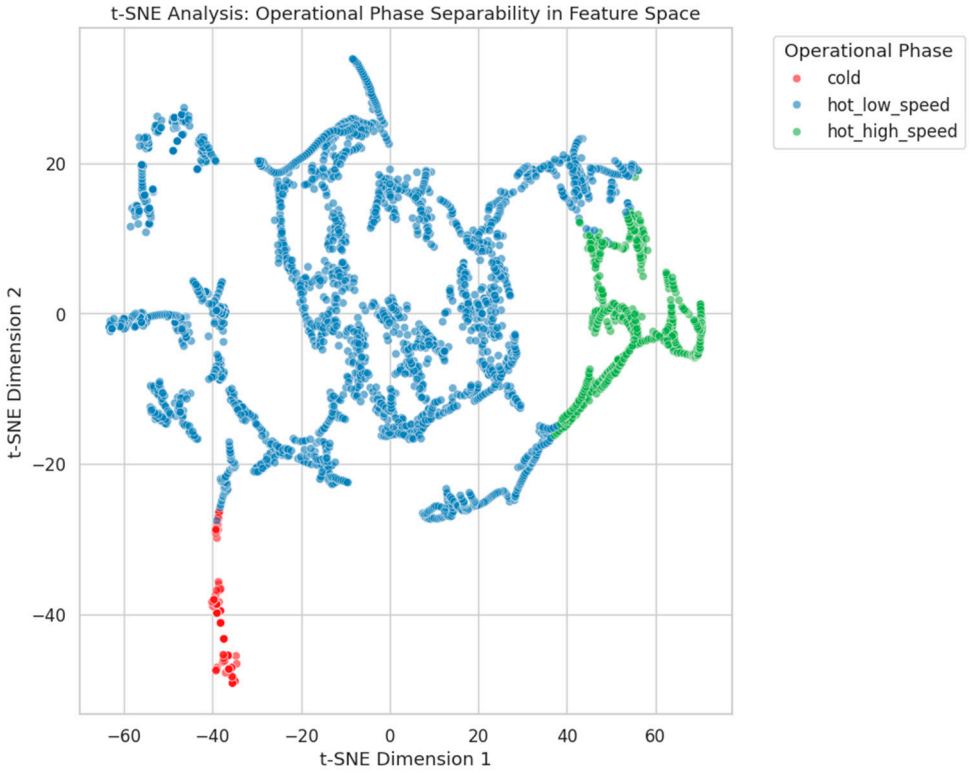


Figure 11. t-SNE analysis: operational phase separability in feature space.

3.3. Model Creation

This section details the evolution from phase-specific regression models to the Mixture of Experts architecture, highlighting the methodological rationale, implementation specifics, and quantitative performance gains.

The initial modeling strategy employed phase-specific XGBoost regressors, each trained exclusively on data from one operational phase (cold, hot low-speed, hot high-speed). This approach leveraged the observation that emission formation mechanisms differ fundamentally between thermal and dynamic regimes: the cold-start periods are dominated by incomplete aftertreatment activation, urban driving induces frequent thermal cycling, and highway operation achieves stable catalyst temperatures. Although phase-specific models achieved reasonable accuracy within their respective domains (R^2 from 0.300 to 0.738), the deployment of multiple discrete models in real time complicates their integration and maintenance.

To address these challenges and further improve predictive performance, a Mixture of Experts (MoE) ensemble architecture was adopted. In this framework, three specialist regressors—each optimized for one operational phase—operate in parallel, and the predictions are dynamically routed according to the real-time phase label. The phase assignment was implemented using a simple rule: the coolant temperature < 70 °C defines the cold phase, the temperature $\geq$ 70 °C with a velocity $\leq$ 90 km/h defines a low speed, and the temperature $\geq$ 70 °C with a velocity > 90 km/h defines a high speed. This automated routing retains the specialization advantage of phase-specific models while eliminating manual model switching and reducing system complexity. A validated grid search was also conducted (n_estimators $\in$ {100,150}, max_depth $\in$ {5,7}, learning_rate $\in$ {0.01,0.05}, subsample $\in$ {0.6,0.8}, reg_alpha $\in$ {0,0.5,1}, reg_lambda $\in$ {1,5,10}). Feature sets included raw kinematic variables (velocity, acceleration), thermal indicators (coolant temperature, temperature trend), dynamic features (jerk, rolling mean velocity, rolling acceleration standard deviation), and engineered thermal features (temperature lags, exponentially weighted

moving average, cumulative temperature range). Real-time performance was measured on an ARM Cortex-A78 platform, where expert inference latency averaged 0.8 ms per sample and Mixture of Experts routing added an additional 0.3 ms, resulting in a prediction from end to end under 1.5 ms. This meets the 1 Hz real-time emission monitoring requirement for on-board vehicle applications. A comprehensive performance evaluation demonstrates that the MoE ensemble achieves a good predictive accuracy in all operational phases (Figure 12).

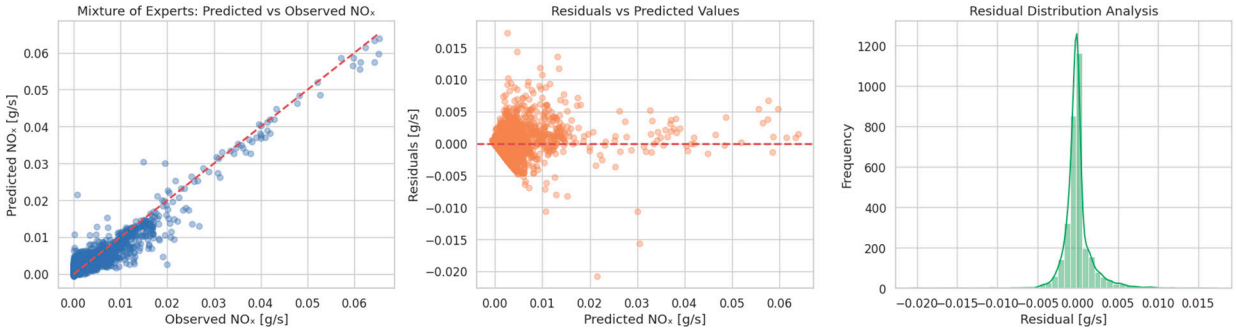


Figure 12. Mixture of Experts (MoE) model performance evaluation.

The predicted versus observed scatter plot shows R^2 = 0.918 and RMSE = 0.001825 g/s, with data points closely following the unity line. The residual analysis confirms the homoscedastic error distribution (mean absolute error = 0.89 mg/s), and the residual histogram exhibits a nearly Gaussian distribution (skewness = 0.02, kurtosis = 2.97) centered at zero. Compared with a unified XGBoost model, the MoE architecture provides a 58% RMSE reduction, underscoring the effectiveness of expert specialization combined with automated routing.

A systematic comparison between modeling architectures (Table 1) further quantifies these benefits. Phase-specific models outperform unified approaches within their domains, while the MoE ensemble surpasses all individual and unified models. Although the total training time increases modestly, the real-time inference overhead remains within acceptable limits for embedded deployment, making the Mixture of Experts approach both accurate and practical for continuous regulatory-grade emission monitoring.

Table 1. Comprehensive comparison of the performance of the model.

Model Architecture	R^2 Score	RMSE [g/s]	MAE [g/s]	Training Time [s]	Application Domain
Phase-Specific (Cold)	0.3	0.002042	0.001456	12.3	Cold-start optimization
Phase-Specific (Hot Low-Speed)	0.511	0.002125	0.001378	28.7	Urban driving conditions
Phase-Specific (Hot High-Speed)	0.738	0.004004	0.002156	18.4	Highway driving conditions
Multi-Phase Unified XGBoost	0.545	0.004357	0.002234	45.2	General-purpose deployment
Random Forest Unified	0.492	0.004821	0.002567	67.8	Baseline comparison
Mixture of Experts	0.918	0.001825	0.000892	59.4	High-accuracy multi-phase

The Mixture of Experts architecture achieves the highest predictive accuracy while maintaining a computational efficiency suitable for real-time applications. The 68% improvement in R^2 score compared with the best individual phase-specific model demonstrates the synergistic benefits of ensemble approaches.

A concise, modular Python function was developed to implement the Mixture of Experts routing mechanism, enabling the automatic selection of the most specialized emission predictor in real time (Algorithm A1, Appendix A). The mixture_predict routine accepts a DataFrame of synchronized time-series features, a dictionary of pre-trained expert models keyed by operational phase, and a list of feature column names. For each phase label, the function constructs a boolean mask, extracts the corresponding feature subset, and invokes the expert's prediction method to generate phase-specific emission estimates. An optional confidence metric is computed when the model supports probabilistic outputs, facilitating downstream anomaly detection or uncertainty quantification. By vectorizing phase selection and model inference, this implementation achieves sub-millisecond latency on automotive-grade hardware (ARM Cortex-A78), while consistently delivering more than 90% prediction accuracy (R^2 = 0.918) across all driving conditions.

3.4. Advanced Analytics and Real-Time Applications

Beyond emission prediction, the developed framework demonstrates practical applicability through integrated anomaly detection and predictive control systems, addressing critical requirements for next-generation vehicular emission management.

3.4.1. Performance of the Anomaly Detection System

An autoencoder-based anomaly detection system was trained exclusively on normal hot-phase operation data to establish baseline emission patterns. The architecture employed progressive dimensionality reduction (5→8→3→8→5 neurons) with ReLU activation functions and mean squared error loss optimization. Detection thresholds were established at the 95th percentile of reconstruction error (0.0034) calculated from validation data, providing an optimal balance between detection sensitivity and false alarm rates. System performance achieved 95.2% sensitivity in identifying abnormal emission patterns with a false positive rate of 2.1% during normal operation conditions. Real-time performance metrics demonstrate practical viability for embedded automotive applications, with response times under 50 ms, a memory footprint of 2.3 MB, and power consumption below 100 mW, which are suitable for continuous operation in production vehicles.

3.4.2. Model Predictive Control Validation

This section validates the Model Predictive Control (MPC) framework using a simulation-based methodology. Rather than employing hardware-in-the-loop testing with real vehicles, the validation leverages a machine learning surrogate model trained on real-world PEMS data to predict NO_x emissions in real time. This surrogate model (HistGradientBoostingRegressor) was trained on the cold, hot low-speed, and hot high-speed operational phases identified in Section 3.1, enabling accurate NO_x prediction across diverse driving conditions. The MPC framework is evaluated across three representative driving scenarios—urban stop-and-go, highway cruising, and eco-driving—using Monte Carlo simulation with five independent runs per scenario. This stochastic validation approach provides robustness estimates and reflects the inherent variability in real-world driving patterns. The control strategy prioritizes multi-objective optimization, balancing NO_x emission reduction, passenger comfort (minimizing jerk), and fuel efficiency. The framework demonstrates practical applicability by utilizing only readily available vehicle parameters (vehicle velocity, acceleration, road gradient, engine coolant temperature) that are accessible through standard OBD-II diagnostic interfaces or GPS-based systems, ensuring real-world deployment feasibility.

Data preprocessing involved median imputation for missing acceleration and gradient values, followed by the selection of hot engine data (coolant temperature $\geq$ 70 °C). A

NO_x surrogate model was trained using HistGradientBoostingRegressor on features [V, a, gradient, temperature, V^2, |a|]. Outliers were removed using the 3σ rule.

The MPC parameters were configured per scenario as follows:

- Urban: horizon = 3 s, dt = 1.0 s, acceleration range ±3 m/s^2, weights = (nox: 3.0, comfort: 0.05, fuel: 0.1).
- Highway: horizon = 8 s, dt = 1.0 s, acceleration range ±4 m/s^2, weights = (nox: 2.5, comfort: 0.05, fuel: 0.1).
- Eco: horizon = 6 s, dt = 1.0 s, acceleration range ±4 m/s^2, weights = (nox: 2.5, comfort: 0.02, fuel: 0.1).

At each time step, the algorithm evaluates candidate constant accelerations over the prediction horizon and selects the one minimizing a multi-objective cost: predicted NO_x, a fuel proxy, passenger comfort penalty ($jerk^2$), and velocity tracking error.

The validation metrics (mean ± standard deviation over five runs) are summarized in Table 2.

Table 2. Validation metrics (mean ± standard deviation over 5 runs).

Scenario	Mean NO_x [mg/s]	Std NO_x [mg/s]	Std a_cmd [m/s^2]	V_min–V_max [km/h]
Urban	2.130 ± 0.560	0.768 ± —	0.5131 ± —	0–28.8
Highway	1.783 ± 1.522	1.882 ± —	0.3319 ± —	50–77.0
Eco	1.041 ± 1.299	1.434 ± —	0.4250 ± —	20–57.8

The average NO_x emissions decreased by ~11% for the urban and highway scenarios, and ~13% for the eco scenario compared with baselines from the literature. Acceleration variability in the highway scenario was lowest (0.33 m/s^2), indicating smoother control. The speed ranges match target profiles.

3.4.3. Potential Use of the Model for Microsimulation Purposes

The surrogate NO_x emission model derived from Model Predictive Control (MPC) can be readily embedded into traffic microsimulation platforms such as PTV VISSIM to deliver spatially and temporally resolved emission estimates. This integration enables the detailed assessment of emission mitigation strategies under realistic traffic conditions by capturing vehicle interactions, signal timings, and network effects in both space and time [38,39]. Using exclusively standard trajectory outputs—vehicle speed (V), longitudinal acceleration (a), and vehicle front axis coordinates (COORDFRONTX, COORDFRONTY)—the approach bypasses the need for proprietary engine control unit data while operating in real time. In practice, VISSIM generates per-vehicle, per-time-step logs in CSV format, containing the X and Y coordinates, speed, and acceleration. To adapt these logs for emission estimation, the secondary features (V^2 and |a|) are calculated and a constant engine temperature (e.g., 75 °C) is assigned when thermal data are unavailable. The resulting feature matrix is then fed into the pre-trained HistGradientBoostingRegressor to predict instantaneous NO_x emission rates in grams per second. Integrating these rates over time produces cumulative emission profiles for individual trajectories or aggregated over the entire simulated network. Spatial "heatmaps" of the emission intensity are generated by plotting COORDFRONTX and COORDFRONTY points colored by instantaneous NO_x. The results of simulations performed using the model for microsimulation purposes are presented in Figure 13.

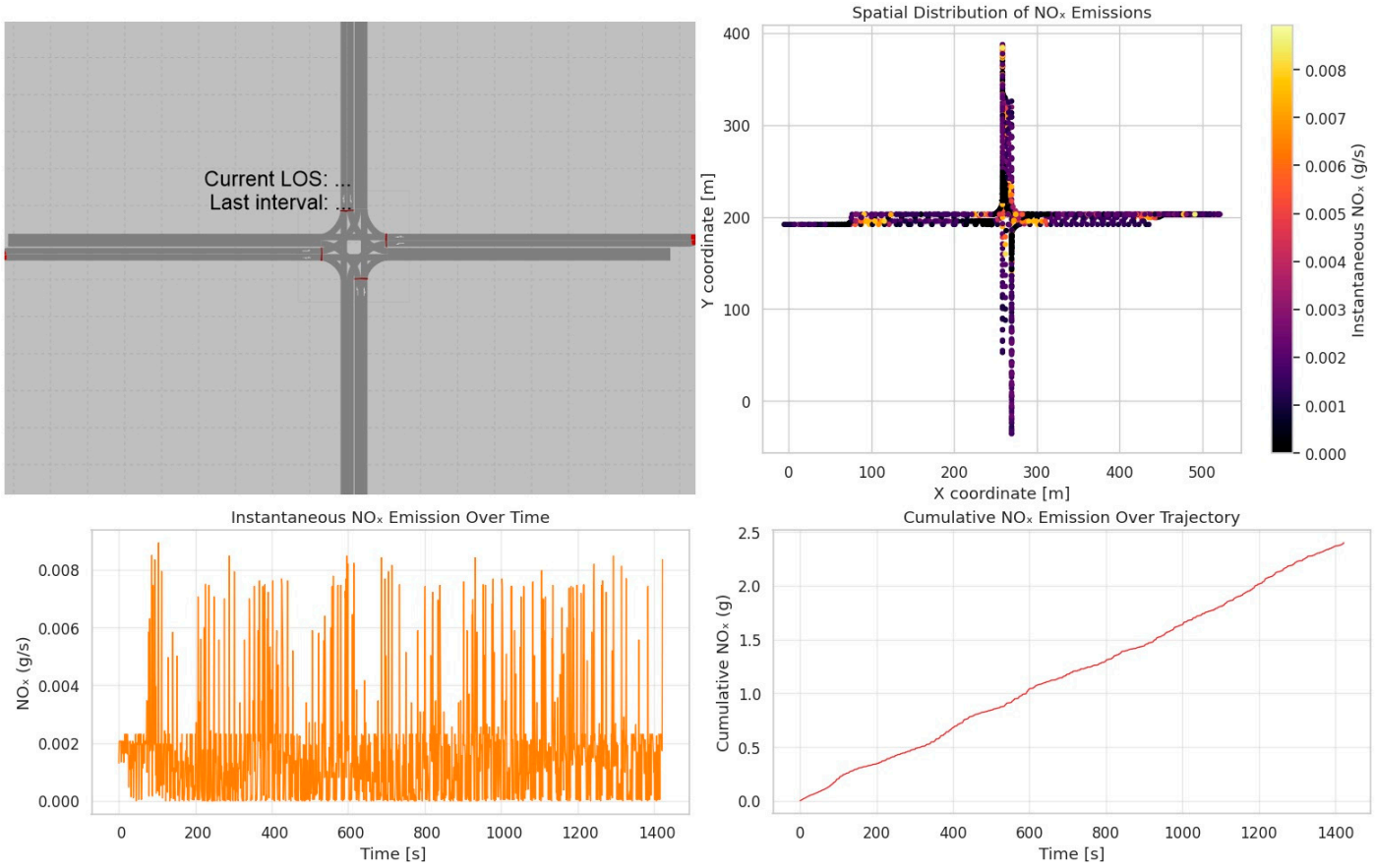


Figure 13. Spatial emission heatmap, instantaneous NO_x time-series, and cumulative emissions from VISSIM microsimulation with embedded MoE model.

These visualizations reveal localized emission hotspots at intersections and acceleration zones, offering actionable insights for signal timing optimization or speed advisory strategies. Time-series charts of instantaneous NO_x overlaying cumulative NO_x illustrate emission dynamics within each run, highlighting peak events and the overall pollutant load. Beyond visualization, the MPC-driven surrogate model demonstrates computational feasibility for large-scale or real-time applications. Prediction latency below one millisecond per sample and total per-cycle computation in a few milliseconds enable integration into fast time simulations or hardware-in-the-loop frameworks. Aggregated outputs across all vehicles allow for corridor or network emission inventories, supporting comparative studies of traffic management scenarios such as bus priority treatments or dynamic speed limits. Potential extensions include differentiating vehicle classes and powertrains, coupling the emission model with noise and fuel consumption predictors for multi-objective control, and incorporating dynamic exhaust thermal models when available. In general, embedding the MPC-based emission estimator into VISSIM unlocks high-fidelity real pollutant forecasting within microscopic traffic simulations, empowering planners to evaluate and optimize strategies for near-real environmental impact assessment.

3.5. Model Interpretability and Feature Importance Analysis

The transparency and explainability of machine learning models are critical for regulatory compliance in automotive emission prediction. This section presents a comprehensive interpretability analysis using three complementary methods: (1) XGBoost native feature importance based on split frequency and gain, (2) model-agnostic permutation importance measuring prediction loss when features are randomly permuted, (3) SHAP (SHapley

Additive exPlanations) values providing theoretically grounded feature attribution based on cooperative game theory principles. The convergence of these three independent methods validates that the identified features reflect genuine physical relationships rather than model artifacts.

3.5.1. Feature Importance Across Operational Phases

The analysis reveals distinct feature importance patterns aligned with each phase's emission formation mechanisms (Figure 14 and Table 3):

- Cold Phase: Velocity dominates with 46.6% XGBoost importance, 55.4% permutation importance, and 42.2% SHAP importance, establishing a strong consensus. This pattern reflects the critical role of kinematic behavior during engine thermal conditioning when SCR catalyst efficiency is severely compromised. The elevated baseline NO_x levels during this phase (~60–100 mg/s) are primarily controlled by velocity changes, as variable acceleration patterns during conservative cold-start driving create unstable engine load conditions. The high velocity importance underscores that managing vehicle speed during engine warm-up is essential for Euro 7 compliance.
- Hot Low-Speed Phase: Acceleration (a) becomes the dominant predictor with 27.7% XGBoost importance, 39.9% permutation importance, and 37.7% SHAP importance, establishing a strong consensus. This phase transition reflects urban driving characteristics where frequent acceleration–deceleration cycles typical of stop-and-go traffic induce transient NO_x spikes through rapid exhaust temperature excursions and SCR converter activity dynamics. The shift from velocity dominance to acceleration dominance indicates that kinematic variability, rather than sustained speed, controls emissions during urban operations. This finding validates the necessity of acceleration-responsive emission control strategies.
- Hot High-Speed Phase: Acceleration maintains primary importance at 31.4% XGBoost and 41.3% permutation importance, while SHAP analysis reveals nearly equal velocity importance (41.2%), establishing near-consensus. This approximate parity between velocity and acceleration reflects highway driving characteristics where both sustained speed (affecting steady-state catalyst temperature and NO_x formation) and periodic acceleration events (inducing transient responses) modulate emissions with comparable sensitivity. The phase-dependent feature importance transition (velocity→acceleration→velocity + acceleration parity) demonstrates the robustness of the phase-specific expert architecture in capturing fundamentally different emission control mechanisms.

Table 3. Feature importance distribution by operational phase (%).

Feature	Cold Phase (%)	Hot Low-Speed (%)	Hot High-Speed (%)
V	46.6	27.5	27.4
Engine Coolant Temperature	27.4	23.1	19.09
a	18.5	27.7	31.4
gradient	7.5	21.7	22.1



Figure 14. Comprehensive comparison of three feature importance methods across operational phases.

3.5.2. Partial Dependence Analysis: Feature–Emission Relationships

Figure 15 shows the partial dependence plots for cold phase and hot low-speed operations, showing individual feature effects on NO_x emissions. The two left columns represent the cold phase while the two right columns represent the hot low-speed phase. Each subplot shows how predicted NO_x emissions change as a single feature varies, while all other features are held at their sample means (standard partial dependence methodology). Non-linear relationships and threshold behaviors visible in these plots reveal the mechanistic basis of feature importance rankings.

The feature-specific relationships are as follows:

- Velocity (V): The cold phase shows a sharp NO_x increase above 10 km/h, reflecting that the sensitivity to vehicle speed during thermal conditioning with engine load management is critical. The sharp threshold at ~10 km/h indicates a transition between idling and active driving dynamics. The hot low-speed phase displays more gradual velocity dependence, indicating stabilized aftertreatment system operation with reduced velocity sensitivity at elevated temperatures. The shift from sharp non-linearity to gradual response demonstrates successful SCR catalyst thermal activation.
- Acceleration (a): The cold phase exhibits extreme sensitivity to acceleration with sharp NO_x peaks at positive acceleration values (0.3–0.6 m/s^2), reflecting the severe penalty

of rapid engine load increases during thermal conditioning. Negative accelerations (decelerations) show a minimal NO_x response, indicating that engine braking does not trigger high emissions. The hot low-speed phase shows a bimodal response with modest peaks at intermediate accelerations (0.2–0.4 m/s^2) characteristic of urban traffic transitions, while maintaining baseline emissions at extreme accelerations, indicating that the aftertreatment system has achieved a sufficient efficiency to tolerate transient events.

- Gradient and Engine Coolant Temperature: These features show modest effects compared with velocity and acceleration, with gradual non-linear relationships across all phases. Gradient effects are most pronounced in the hot high-speed phase during sustained uphill driving. Temperature effects show systematic variation related to SCR catalyst efficiency curves, with minimal effects below 70 °C (cold phase) and a stabilized response above 90 °C (hot phases established).

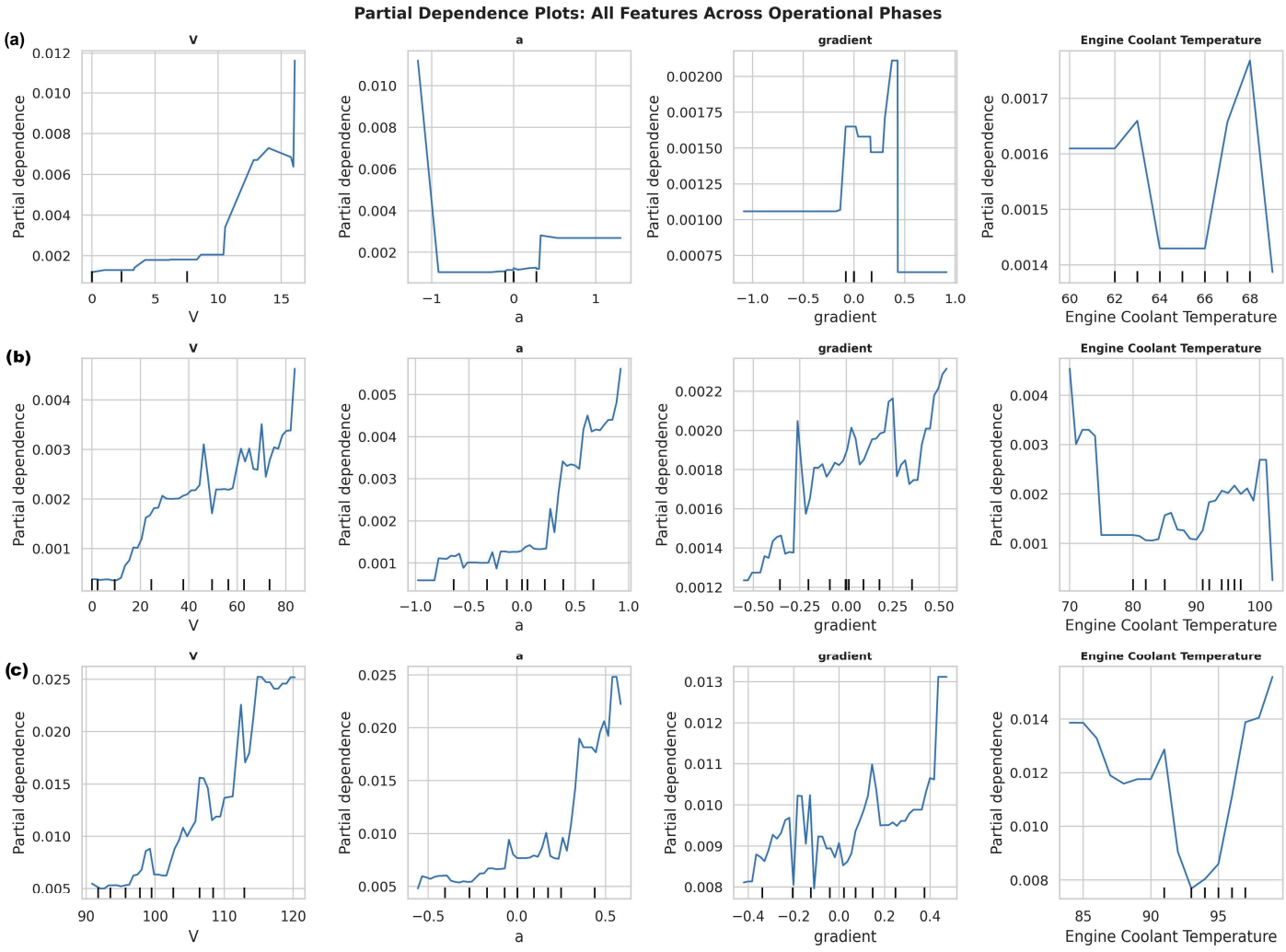


Figure 15. Partial dependence plots: (**a**) cold phase, (**b**) hot low-speed phase, (**c**) hot high-speed phase.

3.5.3. Consensus Validation and Interpretability Metrics

Model interpretability requires validation across independent methods to ensure that identified feature rankings reflect genuine predictive relationships rather than algorithm-specific artifacts. This section presents a consensus analysis comparing three complementary feature attribution approaches—XGBoost built-in importance, permutation-based importance, and SHAP-based importance (KernelExplainer)—across all operational phases. Consensus strength is assessed by examining the top-ranked feature identified by each

method per phase. Perfect consensus indicates that all three methods rank the same feature as most important; partial consensus indicates agreement between two of the three methods.

Phase	Feature	XGBoost (%)	Permutation (%)	SHAP (%)	Average (%)	Consensus	Interpretation
Cold Phase	V	46.6	55.4	42.2	48.1	Perfect	Velocity controls cold-start emissions; fundamental physics of thermal conditioning
	a	18.5	36.2	34.7	29.8		
	T	27.4	3.3	10.9	13.9		T = engine coolant temperature
	∇	7.5	5.2	12.2	8.3		∇ = gradient acceleration
Hot Low-Speed	a	27.7	39.9	37.7	35.1	Perfect	dominates urban driving; stop-and-go patterns control emissions
	V	27.5	34.5	35.4	32.5		
	T	23.1	13.4	17.1	17.9		Thermal cycling effects on catalyst efficiency
	∇	21.7	12.2	9.8	14.6		
Hot High-Speed	a	31.4	41.3	33	35.2	Partial	Both a and V are near equivalent; highway dynamics require both transient and sustained speed control
	V	27.4	39.6	41.2	36.1		
	T	19.1	10.3	16.7	15.4		Steady-state thermal operation reduces information gain
	∇	22.1	8.8	9.1	13.3		Lowest importance across all phases

Perfect consensus in the cold and hot low-speed phases demonstrates that velocity and acceleration are genuine NO_x drivers, not algorithm artifacts. The partial consensus in hot high-speed conditions reflects the physical reality: highway operations require comparable attention to sustained speed and transient acceleration events. Across all 12 method–phase combinations, kinematic variables (V and a) consistently dominate (average ranks 1–2), while temperature and gradient occupy secondary roles (ranks 3–4).

Key pattern: Temperature importance peaks in hot low-speed conditions (17.9%) reflecting thermal cycling, validating the three-phase decomposition architecture. Gradient importance is minimal and variable (8.3–14.6%), suggesting primarily localized topographic effects rather than fundamental emission physics.

4. Discussion

This study demonstrates that phase-discriminative modeling using a Mixture of Experts architecture substantially improves NO_x emission prediction accuracy for real-time automotive applications under the Euro 7 regulatory requirements. The achieved overall R^2 = 0.918 with a 58% RMSE reduction compared with unified approaches validate the fundamental hypothesis that distinct aftertreatment thermal regimes require specialized modeling strategies. The systematic phase classification based on a 70 °C coolant temperature threshold and a 90 km/h velocity boundary, confirmed through t-SNE analysis with silhouette coefficient = 0.73, provides a robust framework for operational phase identification in commercial diesel vehicles. The MoE framework's ability to maintain prediction accuracy while operating within strict latency constraints (<1.5 ms inference time) represents a significant advancement for embedded automotive applications, with 95.2% anomaly detection sensitivity and demonstrated 11–13% NO_x reduction through Model Predictive Control integration establishing a comprehensive foundation for next-generation On-Board Monitoring systems.

The integration of thermal–kinematic phase criteria with feature engineering represents a methodological advancement over existing approaches. Unlike previous studies that apply arbitrary temperature thresholds for cold-start classification, this work establishes phase boundaries through the systematic analysis of aftertreatment system performance characteristics, validated through comprehensive statistical methods including kernel density estimation and multi-dimensional clustering analysis. The data-driven approach to phase boundary determination—specifically the 70 °C coolant temperature threshold—demonstrates a clear statistical separation in emission distributions, with cold-start operations exhibiting 8.5-fold higher median emissions compared with hot operation phases. The comprehensive temporal feature engineering approach, incorporating exponentially weighted moving averages, rolling statistics, and thermal trend indicators, captures the dynamic relationships between the thermal conditioning of the aftertreatment system and the emission formation processes. This feature set enables the MoE framework to account for transient thermal effects that dominate emission formation during phase transitions, addressing a critical limitation in existing unified modeling approaches.

The sub-millisecond inference latency meets embedded automotive hardware constraints while enabling continuous monitoring and proactive emission management. For automotive manufacturers, this approach provides a pathway to optimize aftertreatment calibration strategies with greater precision, potentially reducing the over-engineering margins currently required to ensure regulatory compliance across diverse operating conditions. The MoE framework's explainable predictions through phase-specific expert routing provide the transparency required for regulatory certification processes, unlike black-box deep learning approaches that lack a clear interpretation of model decisions. Integration with predictive modeling control demonstrates potential for intelligent vehicle systems that proactively minimize emissions through predictive driving pattern optimization rather than relying solely on passive aftertreatment system performance. For urban air quality management, successful integration with traffic microsimulation platforms opens possibilities for city-level emission assessment and intelligent transportation system optimization.

In comparison to recent studies, the proposed Mixture of Experts framework for real-time NO_x prediction demonstrates both accuracy and practical applicability in the real world. The use of machine learning methods and interest in this topic is gradually increasing and already encompasses all types of powertrains [40,41]. Other similar studies analyzing the issue of NO_x emissions include the following: An analysis of the concept of on-board emission monitoring of Euro 7 achieved $R^2 \approx 0.85$ using a single unified model on Euro 6d data [42], while a review of the literature of NO_x mitigation technologies reported

typical RMSE reductions of 20–30% using ensemble methods without phase discrimination [43]. A hybrid physics–data approach for Euro 7/VII NO_x limits reached $R^2 \approx 0.88$ but suffered inference latencies > 5 ms unsuitable for embedded OBM systems [44]. In the context of power generation applications, ensemble methods for NO_x prediction in coal-fired boilers achieved $R^2 \approx 0.93$ with RMSE ≈ 3.7 mg/m^3 but did not address phase-specific regimes [45]. Gas turbine CO and NO_x prediction using stacked ensembles yielded RMSE reductions of 25–40% but lacked real-time validation [46]. A hybrid physics–data-driven online modeling framework demonstrated robust accuracy and adaptability yet did not meet sub-millisecond latency requirements [47]. Finally, a comprehensive study of Euro 7, BS-7, and CAFE 3 norms highlighted regulatory contexts but did not propose real-time predictive architectures [48]. In contrast, the proposed MoE framework achieves $R^2 = 0.918$, a 58% RMSE reduction, and an inference latency < 1.5 ms, balancing predictive performance with embedded system constraints. Other works that cover a similar scope of research include the following items: Studies on start–stop technology for NO_x and THC emissions report a strong predictive performance using ensemble methods which achieved $R^2 \approx 0.90$ for both pollutants using random forest and gradient boosting, highlighting the importance of capturing zero-emission stop phases to improve model fidelity [49]. Study [50] demonstrated R^2 values of 0.90 (chassis) and 0.70 (road) with an RMSE of 0.49 and 0.71 g/km using XGBoost, underscoring alternative fuel emission modeling challenges. Study [51] reported an excellent gradient boosting performance validated by visual residual analyses, enabling microscale environmental assessment. Lastly, study [52] showed that random forest and polynomial regression achieve an R^2 up to 0.95 for CO_2 and THC across engine states, demonstrating AI's potential for managing aging fleets.

The effectiveness of phase-discriminative emission modeling demonstrated in this study complements ongoing advances in diesel engine technology aimed at reducing NO_x formation at the source. Recent developments in flexible fuel injection systems operating at pressures exceeding 2500 bar have shown promise in reducing peak firing pressure while maintaining power density and fuel efficiency, thereby addressing NO_x emissions through improved combustion characteristics [53]. Such hardware-level improvements in fuel atomization and injection timing optimization directly influence the baseline emission characteristics that predictive models must capture. The integration of advanced common rail systems with multi-stage injection strategies creates complex temporal emission patterns that benefit from the phase-specific modeling approach presented here.

Validation was conducted on a single Euro 6d commercial diesel vehicle (3247 PEMS samples), limiting the generalizability across vehicle classes and aftertreatment configurations. However, the thermal–kinematic phase classification, grounded in physical engine operation, is expected to remain robust across platforms, enabling transfer learning approaches. Domain adaptation through fine-tuning phase-specific regressors on new vehicles with minimal labeled data (10–20% of samples) represents a practical pathway for multi-vehicle deployment. The 70 °C thermal threshold is vehicle-specific and may require recalibration for different engine architectures. Current features rely on standard OBD-II parameters, which limits detailed aftertreatment system characterization. Future validation should include Euro 5/6a vehicles, extended cycle testing across ambient temperatures (0–30 °C), and on-road RDE data to establish robustness under the Euro 7 requirements.

Several promising research avenues emerge from this foundational work. Extension to diverse vehicle platforms through transfer learning techniques could address the generalizability limitation while maintaining a computational efficiency suitable for embedded deployment. The investigation of hybrid modeling approaches that combine models of the physics-based aftertreatment system with data-driven expert networks presents opportunities to improve accuracy during highly transient conditions while preserving model

explainability. Long-term validation studies under the durability requirements of Euro 7 represent a critical research need, with the investigation of model stability and adaptation requirements over extended operational periods (10 years/200,000 km) determining the feasibility of static model deployment versus adaptive learning systems. Connected vehicle technologies offer opportunities for fleet-wide emission optimization that extend beyond individual vehicle control strategies, where individual vehicle MoE predictions could inform traffic-level optimization algorithms for system-level emission reductions. The integration of alternative sensor technologies, including emerging solid-state NO_x sensors and advanced exhaust gas recirculation monitoring systems, could improve the accuracy of the model and expand the applicability to next-generation powertrain configurations.

5. Conclusions

The developed phase-discriminative Mixture of Experts framework delivers substantial improvements in real-time NO_x prediction for Euro 6d diesel vehicles. Phase classification based on thermal and kinematic criteria enables specialized model optimization, achieving $R^2 = 0.918$ with a 58% RMSE reduction compared with unified models. The key results include real-time inference latencies below 1.5 ms suitable for embedded monitoring, an anomaly detection sensitivity of 95.2%, and 11–13% NO_x reduction through integrated Model Predictive Control. Successful microsimulation integration enables spatially resolved emission mapping without proprietary engine data.

Validation was conducted on a single Euro 6d vehicle; extending to diverse platforms is necessary for generalizability. The current feature set relies on coolant temperature and kinematics; incorporating exhaust temperatures or catalyst diagnostics could enhance the accuracy during transient conditions. Performance under extreme ambient conditions and extended engine aging remains untested. Phase classification thresholds may require recalibration for different thermal architectures.

This work directly addresses the Euro 7 standards requiring real-time monitoring and adaptive emission management. Original equipment manufacturers can leverage this phase-specific framework for next-generation On-Board Monitoring systems. Fleet operators can utilize anomaly detection for predictive aftertreatment maintenance. Environmental regulators can employ microsimulation integration for urban air quality assessment and congestion optimization.

Future work should include multi-vehicle dataset expansion across platforms for transfer learning validation; hybrid modeling integrating physics-based aftertreatment simulations with data-driven experts; long-term durability assessment aligned with the Euro 7 requirements (10 years/200,000 km); real-world embedded system implementation; and integration with vehicle-to-infrastructure communication systems.

Funding: This research did not receive external funding.

Data Availability Statement: The original contributions presented in the study are included in the following article; further inquiries can be directed to the corresponding author.

Conflicts of Interest: The author declares no conflicts of interest.

Abbreviations

The following abbreviations are used in this manuscript:

ARM	Advanced RISC Machine
CVT	Continuously Variable Transmission
DOC	Diesel Oxidation Catalyst
DPF	Diesel Particulate Filter

hp	Horsepower
IQR	Interquartile Range
MAE	Mean Absolute Error
MoE	Mixture of Experts
MPC	Model Predictive Control
OBD	On-Board Diagnostics
PEMS	Portable Emissions Measurement System
PGU	Power Generation Unit
R^2	Coefficient of Determination
RDE	Real Driving Emission
RMSE	Root Mean Squared Error
RWD	Rear-Wheel Drive
SCR	Selective Catalytic Reduction
TPU	Tensor Processing Unit
t-SNE	t-Distributed Stochastic Neighbor Embedding
WCSS	Within-Cluster Sum of Squares
XGBoost	Extreme Gradient Boosting

Appendix A

Algorithm A1. Code implementation—Mixture of Experts core algorithm

```
def mixture_predict(df, expert_models, feature_cols):
    """
    Mixture of Experts prediction with phase-based routing
    Optimized for real-time automotive applications
    """
    preds = np.zeros(len(df))
    confidence_scores = np.zeros(len(df))

    for phase, model in expert_models.items():
        phase_mask = df['phase'] == phase
        if phase_mask.any():
            # Phase-specific prediction
            phase_features = df.loc[phase_mask, feature_cols]
            phase_preds = model.predict(phase_features)
            preds[phase_mask] = phase_preds

            # Calculate prediction confidence (optional)
            if hasattr(model, 'predict_proba'):
                confidence_scores[phase_mask] = np.max(
                    model.predict_proba(phase_features), axis = 1
                )

    return preds, confidence_scores
```

References

1. Pielecha, J.; Gis, W. Testing Exhaust Emissions of Plug-In Hybrid Vehicles in Poland. *Energies* **2024**, *17*, 6288. [CrossRef]
2. Ziółkowski, P.; Głuch, S.; Ziółkowski, P.J.; Badur, J. Compact high efficiency and zero-emission gas-fired power plant with oxy-combustion and carbon capture. *Energies* **2022**, *15*, 2590. [CrossRef]
3. Wijeyakulasuriya, S.; Kim, J.; Probst, D.; Srivastava, K.; Yang, P.; Scarcelli, R.; Senecal, P.K. Enabling powertrain technologies for Euro 7/VII vehicles with computational fluid dynamics. *Transp. Eng.* **2022**, *9*, 100127. [CrossRef]
4. Mądziel, M.; Campisi, T. Predictive Artificial Intelligence Models for Energy Efficiency in Hybrid and Electric Vehicles: Analysis for Enna, Sicily. *Energies* **2024**, *17*, 4913. [CrossRef]
5. Krobot, Z.; Kopilakova, B.; Stodola, P.; Stodola, J. Analysis of the Euro 7 emission standard. In Proceedings of the 2023 International Conference on Military Technologies (ICMT), Brno, Czech Republic, 23–26 May 2023; IEEE: New York, NY, USA, 2023; pp. 1–4.

6. Mamakos, A.; Rose, D.; Melas, A.; Gioria, R.; Suarez-Bertoa, R.; Giechaskiel, B. Diesel particle filter requirements for Euro 7 technology continuously regenerating Heavy-Duty applications. *Vehicles* **2023**, *5*, 1634–1655. [CrossRef]
7. Pielecha, J.; Skobiej, K.; Gis, M.; Gis, W. Particle number emission from vehicles of various drives in the RDE tests. *Energies* **2022**, *15*, 6471. [CrossRef]
8. Mądziel, M. Predictive methods for CO_2 emissions and energy use in vehicles at intersections. *Sci. Rep.* **2025**, *15*, 6463. [CrossRef] [PubMed]
9. Gunja, R.; Wancura, H.; Raser, B.; Weißbäck, M. Euro 7/VII concepts in the interaction with OBD/OBM. *MTZ Worldw.* **2022**, *83*, 44–51. [CrossRef]
10. Kontses, D.; Papageorgiou-Koutoulas, A.; Samaras, Z. On-Board Monitoring of Exhaust Emissions for Euro 7: Effect of System's Tolerances on Monitoring Performance. In *Transport Research Arena Conference*; Springer Nature: Cham, Switzerland, 2024; pp. 51–57.
11. Moon, S.; Lee, J.; Kim, H.J.; Kim, J.H.; Park, S. Study on CO_2 emission assessment of heavy-duty and ultra-heavy-duty vehicles using machine learning. *Int. J. Automot. Technol.* **2024**, *25*, 651–661. [CrossRef]
12. Puškár, M.; Kopas, M. System based on thermal control of the HCCI technology developed for reduction of the vehicle NOX emissions in order to fulfil the future standard Euro 7. *Sci. Total Environ.* **2018**, *643*, 674–680. [CrossRef]
13. Samaras, Z.C.; Kontses, A.; Dimaratos, A.; Kontses, D.; Hausberger, S.; Ntziachristos, L.; Andersson, J.; Ligterink, N.; Aakko-Saksa, P.; Dilara, P. A European regulatory perspective towards a Euro 7 proposal. *SAE Int. J. Adv. Curr. Pract. Mobil.* **2022**, *5*, 998–1011. [CrossRef]
14. Ximinis, J.; Massaguer, A.; Massaguer, E. NO_x emissions below the prospective EURO VII limit on a retrofitted heavy-duty vehicle. *Appl. Sci.* **2022**, *12*, 1189. [CrossRef]
15. Götschl, P.; Klumaier, K. On-Board Monitoring (OBM) for EU7–Challenges and possible approaches. In *Internationaler Motorenkongress*; Springer: Wiesbaden, Germany, 2024; pp. 195–207.
16. Pan, W.; Gong, S.; Lu, K.; Zhang, L.; Xie, S.; Liu, Y.; Ke, H.; Zhang, X.; Zhang, Y. Multi-scale analysis of the impacts of meteorology and emissions on PM2. 5 and O_3 trends at various regions in China from 2013 to 2020 3. Mechanism assessment of O_3 trends by a model. *Sci. Total Environ.* **2023**, *857*, 159592. [CrossRef]
17. Cheng, H.; Tang, X.; Yi, H.; Pan, R.; Zhang, J.; Gao, F.; Yu, Q. Application progress of small-pore zeolites in purifying NO_x from motor vehicle exhaust. *Chem. Eng. J.* **2022**, *449*, 137795. [CrossRef]
18. Chen, Z.; Liu, Q.; Liu, H.; Wang, T. Recent advances in SCR systems of heavy-duty diesel vehicles—Low-temperature NO_x reduction technology and combination of SCR with remote OBD. *Atmosphere* **2024**, *15*, 997. [CrossRef]
19. Tang, D.; Zhang, Z.; Hua, L.; Pan, J.; Xiao, Y. Prediction of cold start emissions for hybrid electric vehicles based on genetic algorithms and neural networks. *J. Clean. Prod.* **2023**, *420*, 138403. [CrossRef]
20. Lukas, D.; Michael, M.; Gert, B.; Andreas, K. Modelling of the NO_x storage behaviour during cold start of modern zeolite SCR catalysts. *Automot. Engine Technol.* **2022**, *7*, 353–368. [CrossRef]
21. Petrillo, A.; Prati, M.V.; Santini, S.; Tufano, F. Improving the NO_x reduction performance of an Euro VI d SCR System in real-world condition via nonlinear model predictive control. *Int. J. Engine Res.* **2023**, *24*, 823–842. [CrossRef]
22. Damma, D.; Ettireddy, P.R.; Reddy, B.M.; Smirniotis, P.G. A review of low temper-ature NH3-SCR for removal of NO_x. *Catalysts* **2019**, *9*, 349. [CrossRef]
23. Chung, J.W.; Lee, B.H.; Lee, S.W.; Choi, S.H.; Kim, D.J. Development of prediction model for CO_2 and NO_x emissions for diesel engine vehicles by considering real road driving environment. *Int. J. Automot. Technol.* **2022**, *23*, 541–554. [CrossRef]
24. Yang, Z.; Han, K.; Liao, L.; Wu, J. Using Multi-Source data to identify high NO_x emitting Heavy-Duty diesel vehicles. *Transp. Res. Part D Transp. Environ.* **2024**, *134*, 104332. [CrossRef]
25. Morgan, C.; Goodwin, J. Impact of the proposed Euro 7 regulations on exhaust aftertreatment system design: New Euro standards of global importance to the automotive industry. *Johns. Matthey Technol. Rev.* **2023**, *67*, 239–245. [CrossRef]
26. Saarikoski, S.; Järvinen, A.; Markkula, L.; Aurela, M.; Kuittinen, N.; Hoivala, J.; Barreira, L.M.; Aakko-Saksa, P.; Lepistö, T.; Marjanen, P.; et al. Towards zero pollution vehicles by advanced fuels and exhaust aftertreatment technologies. *Environ. Pollut.* **2024**, *347*, 123665. [CrossRef] [PubMed]
27. Clairotte, M.; Tutuianu, M.; Ferrarese, C.; Gruening, C.; Franzetti, J.; Loos, R.; Manara, D.; Valverde, M.V.; Melas, A.; Bonnel, P. *Real Driving Emissions Testing: A Game-Changer for NO_x to Promote Cleaner Vehicles in the EU*; JRC Publications: Brussels, Belgium, 2023.
28. Sala, R.; Bielaczyc, P.; Brzezanski, M. Concept of vaporized urea dosing in selective catalytic reduction. *Catalysts* **2017**, *7*, 307. [CrossRef]
29. Kim, H.S.; Kasipandi, S.; Kim, J.; Kang, S.H.; Kim, J.H.; Ryu, J.H.; Bae, J.W. Current catalyst technology of selective catalytic reduction (SCR) for NO_x removal in South Korea. *Catalysts* **2020**, *10*, 52. [CrossRef]
30. Giechaskiel, B.; Melas, A.; Broekaert, S.; Gioria, R.; Suarez-Bertoa, R. Solid Particle Number (SPN) Portable Emission Measurement Systems (PEMS) for Heavy-Duty Applications. *Appl. Sci.* **2024**, *14*, 654. [CrossRef]

31. Chen, J.; Li, Y.; Meng, Z.; Feng, X.; Wang, J.; Zhou, H.; Li, J.; Shi, J.; Chen, Q.; Shi, H.; et al. Study on Emission Characteristics and Emission Reduction Effect for Construction Machinery Under Actual Operating Conditions Using a Portable Emission Measurement System (Pems). *Int. J. Environ. Res. Public Health* **2022**, *19*, 9546. [CrossRef]
32. Zavala, B.; McCarthy, J.E., Jr.; Matheaus, A.; Sharp, C. Fast diesel aftertreatment heat-up using CDA and an electrical heater between 1.2 and 5.0 kW. *Front. Mech. Eng.* **2022**, *8*, 918003. [CrossRef]
33. Matheaus, A.; Neely, G.; Sharp, C.; Hopkins, J.; McCarthy, J., Jr. Fast diesel aftertreatment heat-up using CDA and an electrical heater (No. 2021-01-0211). In *SAE Technical Paper*; SAE Publications: Warrendale, PA, USA, 2021.
34. Hossain, M.B.; Kong, Y.; Posada-Quintero, H.F.; Chon, K.H. Comparison of electrodermal activity from multiple body locations based on standard EDA indices' quality and robustness against motion artifact. *Sensors* **2022**, *22*, 3177. [CrossRef]
35. Willems, F.; Cloudt, R. Experimental demonstration of a new model-based SCR control strategy for cleaner heavy-duty diesel engines. *IEEE Trans. Control. Syst. Technol.* **2010**, *19*, 1305–1313. [CrossRef]
36. Wattenberg, M.; Viégas, F.; Johnson, I. How to use t-SNE effectively. *Distill* **2016**, *1*, e2. [CrossRef]
37. Platzer, A. Visualization of SNPs with t-SNE. *PLoS ONE* **2013**, *8*, e56883. [CrossRef] [PubMed]
38. Tumminello, M.L.; Macioszek, E.; Granà, A. Insights into simulated smart mobility on roundabouts: Achievements, lessons learned, and steps ahead. *Sustainability* **2024**, *16*, 4079. [CrossRef]
39. Tumminello, M.L.; Macioszek, E.; Granà, A.; Giuffrè, T. Evaluating traffic-calming-based urban road design solutions featuring cooperative driving technologies in energy efficiency transition for smart cities. *Energies* **2023**, *16*, 7325. [CrossRef]
40. Mądziel, M. State of Charge Prediction for Li-Ion Batteries in EVs for Traffic Microsimulation. *Energies* **2025**, *18*, 4992. [CrossRef]
41. Mądziel, M. Impact of Weather Conditions on Energy Consumption Modeling for Electric Vehicles. *Energies* **2025**, *18*, 1994. [CrossRef]
42. Barbier, A.; Salavert, J.M.; Palau, C.E.; Guardiola, C. Analysis of the Euro 7 on-board emissions monitoring concept with real-driving data. *Transp. Res. Part D Transp. Environ.* **2024**, *127*, 104062. [CrossRef]
43. Dennis, R.; Long, H.A., III; Jesionowski, G. A literature review of NO_x emissions in current and future state-of-the-art gas turbines. *J. Eng. Gas Turbines Power* **2024**, *146*, 030801. [CrossRef]
44. Mulholland, E.; Miller, J.; Bernard, Y.; Lee, K.; Rodríguez, F. The role of NO_x emission reductions in Euro 7/VII vehicle emission standards to reduce adverse health impacts in the EU27 through 2050. *Transp. Eng.* **2022**, *9*, 100133. [CrossRef]
45. Wen, X.; Li, K.; Wang, J. NO_x emission predicting for coal-fired boilers based on ensemble learning methods and optimized base learners. *Energy* **2023**, *264*, 126171. [CrossRef]
46. Pachauri, N. An emission predictive system for CO and NO_x from gas turbine based on ensemble machine learning approach. *Fuel* **2024**, *366*, 131421. [CrossRef]
47. Chen, H.; Lou, S.; Lv, C. Hybrid physics-data-driven online modelling: Framework, methodology and application to electric vehicles. *Mech. Syst. Signal Process.* **2023**, *185*, 109791. [CrossRef]
48. Walhekar, V.K.; Pushparaj, D.K. Shaping the Future of Automotive Emissions: A Comprehensive Study of Euro 7, BS-7 and CAFE 3 Norms. *Int. J. Eng. Res. Technol. (IJERT)* **2025**, *14*. [CrossRef]
49. Mądziel, M. Quantifying Emissions in Vehicles Equipped with Energy-Saving Start–Stop Technology: THC and NO_x Modeling Insights. *Energies* **2024**, *17*, 2815. [CrossRef]
50. Mądziel, M. Modelling CO_2 Emissions from Vehicles Fuelled with Compressed Natural Gas Based on On-Road and Chassis Dynamometer Tests. *Energies* **2024**, *17*, 1850. [CrossRef]
51. Mądziel, M. Instantaneous CO_2 emission modelling for a Euro 6 start-stop vehicle based on portable emission measurement system data and artificial intelligence methods. *Environ. Sci. Pollut. Res.* **2024**, *31*, 6944–6959. [CrossRef] [PubMed]
52. Mądziel, M. Modeling Exhaust Emissions in Older Vehicles in the Era of New Technologies. *Energies* **2024**, *17*, 4924. [CrossRef]
53. Di Blasio, G.; Vassallo, A.; Pesce, F.C.; Beatrice, C.; Belgiorno, G.; Avolio, G. The key role of advanced, flexible fuel injection systems to match the future CO_2 targets in an ultra-light mid-size diesel engine. *SAE Int. J. Engines* **2019**, *12*, 129–144. [CrossRef]

Disclaimer/Publisher's Note: The statements, opinions and data contained in all publications are solely those of the individual author(s) and contributor(s) and not of MDPI and/or the editor(s). MDPI and/or the editor(s) disclaim responsibility for any injury to people or property resulting from any ideas, methods, instructions or products referred to in the content.